GRADUATE SCHOOL
EAST TENNESSEE STATE UNIVERSITY

Electronic Theses and Dissertations

Student Works

8-2023

Investigation of the Protein Components in a Periplasmic Mechanism Regulating Bacterial Morphology

Alexandra Pulliam
East Tennessee State University

Follow this and additional works at: https://dc.etsu.edu/etd

Part of the Biology Commons, and the Public Health Commons

Investigation of the Protein Components in a Periplasmic Mechanism Regulating Bacterial

Morphology

_____

A thesis

presented to

the faculty of the Department of Health Sciences

East Tennessee State University

In partial fulfillment

of the requirements for the degree

Master of Science in Biology

_____

by

Alexandra Pulliam

August 2023

_____

Dr. Erik Petersen, Chair

Dr. Jennifer Hall

Dr. Bert Lampson

Keywords: cyclic-di-GMP, *Salmonella*, bacterial morphology, STM3615

ABSTRACT

Investigation of the Protein Components in a Periplasmic Mechanism Regulating Bacterial

Morphology

by

Alexandra Pulliam

Salmonella is a leading bacterial cause of foodborne illness worldwide. During a previous study

investigating the enzymes responsible for regulating cyclic-di-GMP concentrations, a mutant in

the cyclic-di-GMP-specific phosphodiesterase STM3615 was identified that displayed a

phenotype characterized by decreased survival on agar plates and a shorter bacterium length. I

was able to determine that the periplasmic domain of STM3615 was responsible for this

phenotype, not the enzymatic phosphodiesterase domain. Based upon a bioinformatic analysis of

the protein, I then hypothesized that the periplasmic domain of STM3615 was interacting with a

periplasmic protein to give rise to this phenotype. To identify this periplasmic protein partner, a

transposon mutagenesis approach was taken to disrupt genes within the STM3615 mutant. Two

mutants, *rcsD* and *yrfG*, within the STM3615 deletion mutant restored the WT phenotype and

require further investigation. RcsD is an important partner of the transcription regulatory protein

RcsB that controls expression of FtsZ, a key player in cell division.

DEDICATION

I dedicate this work to my friends and family who have always supported me through thick and thin. To my incredible parents, Robin and Cary Pulliam, thank you for always pushing me to do my best, always believing in me even though I can make it hard to at times, and never saying no to helping me continue my academic journey. To my siblings, Caroline and Watson Pulliam, thank you for the joy that you bring to my life; I could not imagine life without you. To the Pulliam pets, past and present, but especially Sammy, Sweetpea, and Cooper, who have provided me with the utmost comfort through difficult times. To Haley Handshy, thank you for your incredible council, support, and friendship and for being my best friend. To Emily Owen, thank you for affirming me and allowing me to be my complete self around you. Thank you all. This would not have been possible without you.

TABLE OF CONTENTS

LIST OF TABLES

LIST OF FIGURES

LIST OF ABBREVIATIONS

CFU   Colony-forming unit

Cyclic-di-GMP   Bis-(3'-5')-cyclic dimeric guanosine monophosphate

DGC   Diguanylate cyclase

LB   Luria broth

NTS   Non-typhoidal *Salmonella*

PDE   Phosphodiesterase

WT   Wild-type

CHAPTER 1. INTRODUCTION

Salmonella enterica

Salmonella is a genus of bacteria comprised of Gram-negative, facultative anaerobic bacilli that belong to the *Enterobacteriaceae* family. Most members of the *Salmonella* genus are motile through their use of peritrichous flagella and do not have the ability to form endospores[1]. The *Salmonella* genus is composed of two species: *Salmonella enterica* and *Salmonella bongori*, of which *Salmonella enterica* is further divided into nearly 2,600 serovars distinguished by their pathogenicity[2]. These serovars are grouped into two categories: typhoidal *Salmonella* and non-typhoidal *Salmonella* (NTS)[3]. The estimates for global NTS infections vary widely because of inconsistent reporting, but approximately 93 million infections occur annually with 155,000 deaths[4]. A self-limiting gastroenteritis is the main disease associated with NTS with symptoms including diarrhea, abdominal pain, nausea, and vomiting[5]. Humans typically become infected with NTS through the fecal-oral route from eating contaminated food products[1]. Because of its worldwide effects, further study of *Salmonella* is necessary to lessen disease and improve quality of life.

In order to study *Salmonella* and enteric bacteria in general, *Salmonella enterica* serovar Typhimurium is commonly used as a model organism. *Salmonella* Typhimurium is one of the most widely reported serovars of NTS infection worldwide[6,7]. While *Salmonella* Typhimurium usually causes a self-limiting gastroenteritis in humans typical of NTS, in some strains of mice, a typhoid-like disease appears which allows study of typhoidal *Salmonella* with less risk to researchers[8]. For these reasons, *Salmonella* Typhimurium can be used to study a wide range of processes that probe both bacterial and host-pathogen components.

Bacterial Morphology

Bacteria come in a vast number of shapes and sizes. While the most well-known groups of bacterial morphologies are cocci, bacilli, and spirochetes, there are several other shapes from cells with branched filaments to cells with an hourglass figure and star-shaped cells[9–12]. Each of these shapes have a distinct purpose: to help the cell survive in its environment. Bacteria have had to adapt to nearly every environment on Earth, and because of selective pressures such as nutrient availability and predation evasion, bacteria have adopted different morphologies to thrive. Bacterial morphology seems to be of chief concern as its regulation is strongly conserved.

The peptidoglycan layer of the bacterial cell wall used to be seen as the main determinant of bacterial morphology, but the large system of proteins that assemble and regulate the peptidoglycan layer seem to drive a bacterium's shape[12]. The peptidoglycan layer is present in the majority of bacteria and serves as a flexible composite that gives the cell its integrity and ability to withstand different pressures and growth conditions[13]. There are many proteins that are involved in the building and modifying of the peptidoglycan layer, most notably, in bacilli like *Salmonella*, MreB, an actin-like protein that works to recruit and direct peptidoglycan biosynthesis, interacting to form helical filaments which connect to the cell membrane[12]. MreB has also been shown to be a cell shape-determining protein as its deletion turns bacilli into cocci and sometimes proves fatal as the cell lyses[14,15]. The action of MreB is dynamic and works throughout the bacterial growth cycle[12].

The bacterial growth cycle includes four phases: lag phase, log phase, stationary phase, and death phase. The lag phase occurs when bacteria are introduced to a new medium and increase metabolic output and physical size in preparation for cell division, but there is no increase in cell number in lag phase[16]. Log phase occurs when bacteria are undergoing cell

division and increasing in number exponentially where the most amount of cell growth occurs. Stationary phase occurs when the number of living cells equals the number of dying or dead cells and depends on a number of factors including nutrient availability, oxygen availability, and waste product accumulation. During stationary phase, bacteria employ survival tactics to limit unnecessary metabolic processes[17]. Death phase occurs when the number of dying cells outnumbers the number of living cells. The onset of death phase varies by species, but as cells age, they lose viability regardless of the medium they inhabit[18]. Throughout the entire bacterial growth cycle, cells rely on extracellular signals in order to function optimally in their environment as they transition from stage to stage. Based on these extracellular signals, bacteria enact cell signaling pathways that have cascading effects all throughout the cell including DNA transcription and protein synthesis. Without these signals, the cells are not able to function correctly, and further study into them could elucidate novel antimicrobial therapies and a better understanding of bacterial physiology.

<p align="center">Bis-(3'-5')-cyclic Dimeric Guanosine Monophosphate</p>

Bis-(3'-5')-cyclic dimeric guanosine monophosphate (cyclic-di-GMP) is a second messenger molecule that is present in several bacterial species and regulates multiple processes including motility, biofilm formation, cell cycle regulation, and virulence[19,20]. Cyclic-di-GMP is produced or degraded based on extracellular signals that activate either diguanylate cycles (DGCs) that synthesize cyclic-di-GMP from two GTP molecules using their GGDEF enzymatic domain or phosphodiesterases (PDEs) that degrade cyclic-di-GMP using their EAL enzymatic domain (Fig. 1) [19–22]. Based on the concentration of cyclic-di-GMP within the cell, it will bind to effector proteins that have vast functions including transcriptional regulators, enzymes, and structural proteins, often times regulating a switch between motile and biofilm states[23].
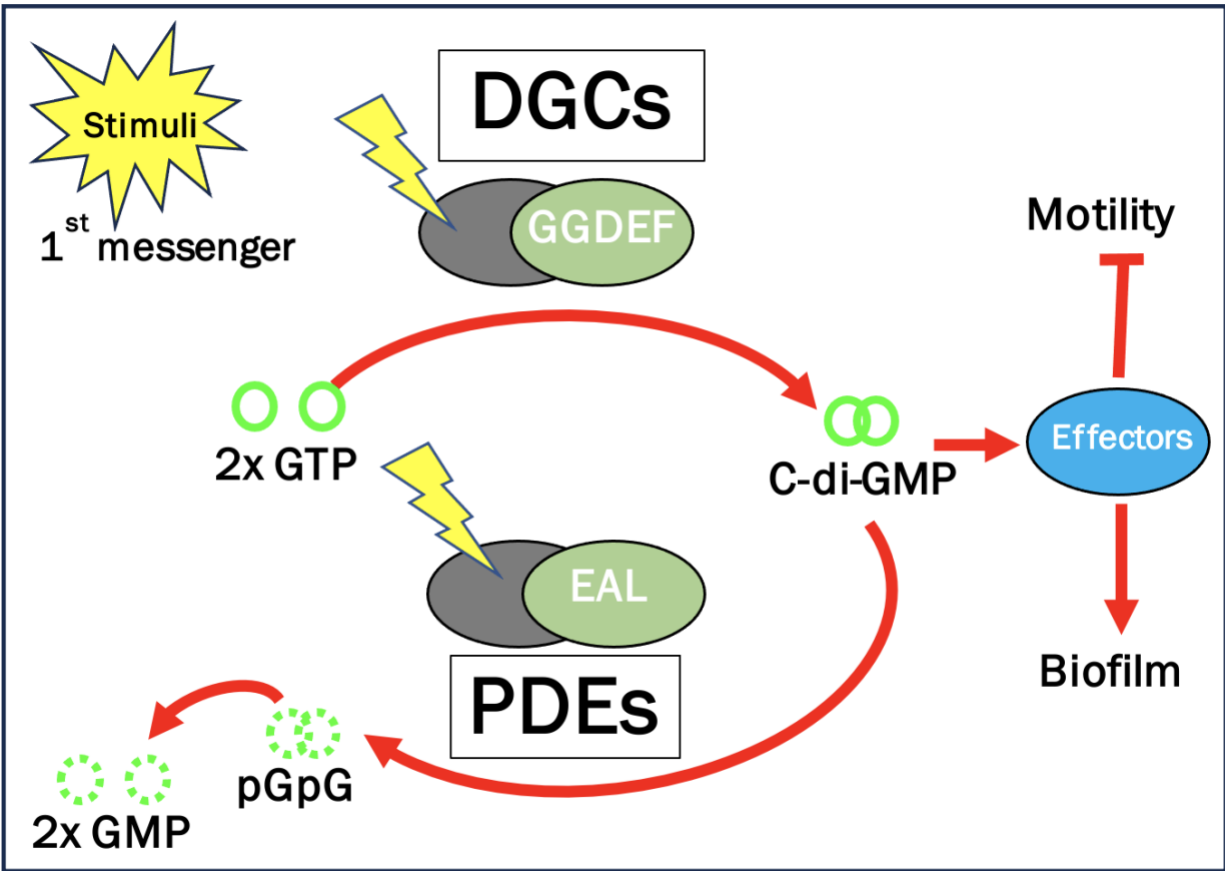
Fig. 1 Cyclic-di-GMP pathway
The bacterial cell detects an extracellular signal called the first messenger. Depending on the first messenger, cyclic-di-GMP will be produced by DGCs from two GTP molecules or degraded by PDEs. The cyclic-di-GMP can then go on to bind effector molecules to regulate a range of phenotypes.

Along with the balance between motility and biofilm, the cyclic-di-GMP pathway has also been shown to be involved in the cell cycle. Specifically, in *Caulobacter*, fluctuating cyclic-di-GMP levels help to coordinate chromosome replication[24]. In *Bacillus anthracis*, cyclic-di-GMP mutants impaired germination kinetics[25]. During starvation, *Myxoccocus xanthus* depends on an essential cyclic-di-GMP increase in the cell to produce spore-filled fruiting bodies for survival[26]. For *Streptomyces*, cyclic-di-GMP helps to regulate both the initiation of development and the differentiation into spores[27]. On the other hand, in *Clostridium difficile*, cyclic-di-GMP

was shown to prevent early sporulation[28]. The vast range of uses the cyclic-di-GMP pathway has

in bacteria opens the door for further study into this complex pathway to discover new regulatory

processes.

<center>STM3615</center>

In *Salmonella* Typhimurium, the cyclic-di-GMP pathway is regulated by 17 proteins that

comprise 6 DGCs, 9 PDEs, and 2 proteins with dual-enzymatic activity[29]. One of the PDEs is a

protein called STM3615 that has an enzymatically active EAL domain, a degenerate GGDEF

domain, a HAMP domain, two transmembrane domains, and a periplasmic domain (Fig. 2) [30].

HAMP domains connect catalytic domains found in the cytoplasm to transmembrane,

periplasmic, and extracellular domains to help transduce signals from outside of the cell to inside

the cell. They work as the mediators between separated protein domains, in this case between the

globular periplasmic domain and the cytoplasmic DGC and PDE domains [31]. While the GGDEF

domain in STM3615 is no longer enzymatically active due to mutations in its active site, it can

still bind cyclic-di-GMP through its I-site[32]. STM3615's EAL phosphodiesterase domain is

likely active at degrading cyclic-di-GMP into the linear pGpG[33].

There have been a few studies into STM3615's role in the pathogenesis of *Salmonella*

Typhimurium. In chickens, an STM3615 mutant was shown to have significantly decreased

colonization of the ceca compared to the wild-type (WT) one day post-infection, while an

STM3615 mutant specifically was cleared from mouse ceca fastest out of 20 cyclic-di-GMP

mutants at about 3 days post infection[34,35]. STM3615 activity has also been shown to be required

for macrophage survival[29]. STM3615 also appears to have a role in biofilm formation as a

combination of a STM3615 mutant and the deletion of the *dsbA-dsbB* periplasmic

<center>17</center>

oxidoreductase system lags the development of the red, dry, and rough morphotype in

Salmonella Typhimurium[36].
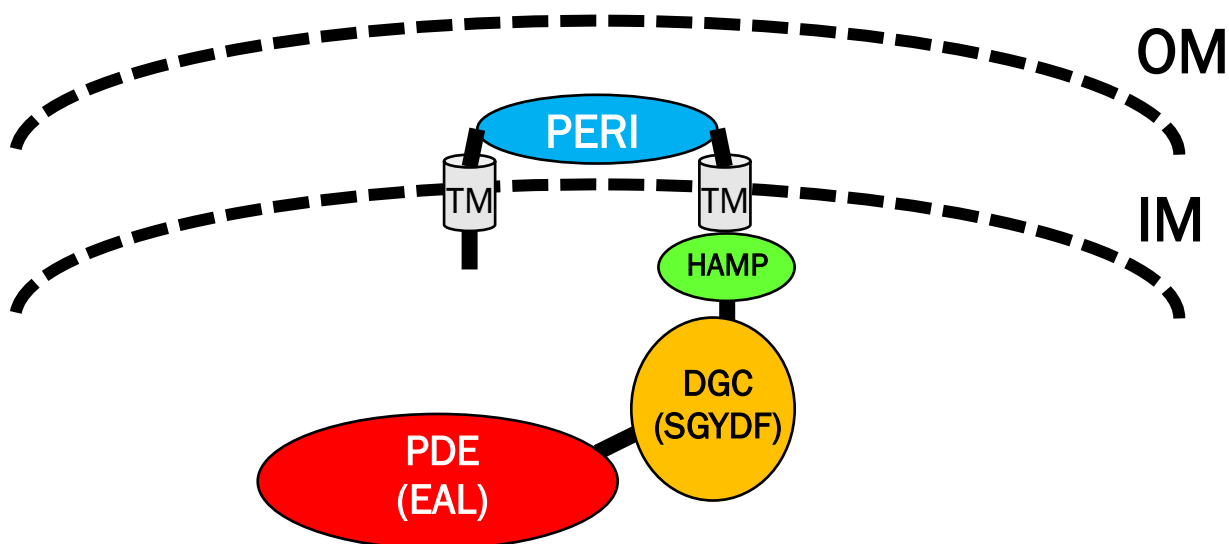
Fig. 2 STM3615 domain organization
STM3615 has six domains: two transmembrane domains with a globular periplasmic domain in
between them, a HAMP domain, a degenerate GGDEF domain, and an enzymatically active
EAL domain.

Previous analysis of a complete STM3615 deletion mutant has sparked some questions.

On a green agar plate meant to monitor phage-induced death of *Salmonella*, the uninfected

STM3615 mutant exhibited a green/blue middle, indicating death, whereas the WT does not.

When examined under a microscope, the STM3615 mutant was observed to have a shorter

bacterial length than its WT counterpart. Here, we determine that these phenotypes appear to be

related to the periplasmic domain of the protein rather than the c-di-GMP phosphodiesterase

activity. Based upon a bioinformatic analysis of the periplasmic domain, I hypothesized that it

has a periplasmic protein partner that gives rise to this phenotype. We elected to set out to

18

discover more about this potential periplasmic partner as its identity could help us in

understanding more about *Salmonella* replication.

CHAPTER 2. MATERIALS AND METHODS

Bacterial Strains and Growth Conditions

All bacterial strains, plasmids, and primers are shown in Appendices A, B, and C, respectfully. Strains were typically grown for 20-24 hours in 2 mL of Luria Broth (LB) at 37ºC shaking at 250 rpm. LB consisted of 10.0 g/L of Fisher BioReagents[TM] tryptone, 5.0 g/L of Fisher BioReagents[TM] yeast extract, and 10.0 g/L of Fisher BioReagents[TM] NaCl. LB plates were made using the LB broth ingredients and 15.0 g/L of Fisher BioReagents[TM] bacteriological agar. Green plates consisted of 7.5 g/L of Fisher BioReagents[TM] dextrose, 1.0 g/L of Fisher BioReagents[TM] yeast extract, 8.0 g/L of Fisher BioReagents[TM] tryptone, 5.0 g/L of Fisher BioReagents[TM] NaCl, 65.0 mg/L of methyl blue, 600.0 mg/L of alizarin yellow, and 15.0 g/L of Fisher BioReagents[TM] bacteriological agar. When needed, gentamicin was added to a concentration of 30 µg/mL, chloramphenicol to a concentration of 34 µg/mL, kanamycin to a concentration of 100 µg/mL, and ampicillin to a concentration of 100 µg/mL. The antibiotic A22 was dissolved in DMSO at a concentration of 10 mg/mL and added to LB agar plates at a concentration of 2 µg/mL. The strains used were stored indefinitely at -80ºC in their original growth medium with their corresponding antibiotic and 20% glycerol as a preservative.

6x6 Drop Plate Method for Colony Forming Unit Quantification

To quantify bacterial growth in the following assays, a previously described 6x6 drop plate method was used in 96-well plates[37]. 200 µL of a bacterial sample is added to the first column of a 96-well plate. For a 5-fold serial dilution, 160 µL of 1x PBS is added to the rest of the row. 40 µL of the bacterial sample is diluted into the second column, 40 µL of the second column sample is diluted into the third column, and so on (Fig. 3). For a 10-fold serial dilution, 180 µL of 1x PBS is added to the rest of the row with 20 µL sample dilutions. 7 µL of the samples in the last

six columns is then pipetted six times onto an LB plate, creating a 6x6 grid. The spots were

allowed to dry onto the LB plate for 20 minutes. In order to ensure that the colonies did not

overgrow and were able to be counted accurately, the plates were incubated overnight at 25℃

(Fig. 4). After the incubation period, a column was counted for colony-forming units (CFUs) that

were then converted to CFU/ml to quantify bacterial growth.
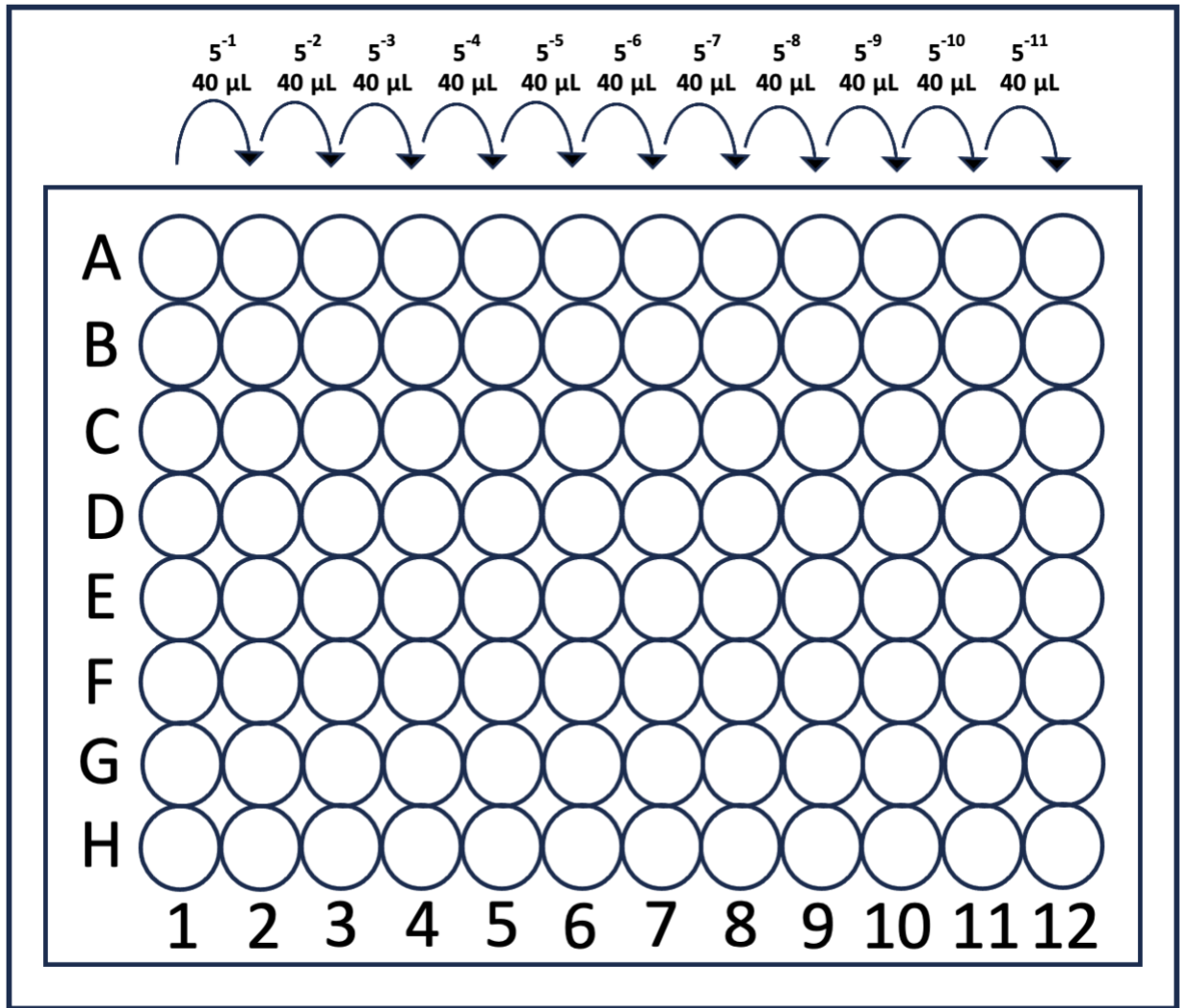
Fig. 3 6x6 drop plate method: 5-fold serial dilution in a 96-well plate
200 µL of a bacterial sample was pipetted into the first column of a 96-well plate. 160 µL of 1x
PBS was pipetted into the wells of the remaining columns. 40 µL of the bacterial sample was
pipetted from the first column into the second column, mixed, and the pipette tip discarded. This
process was repeated for the remaining columns. The last six columns used were plated for
colony counting.
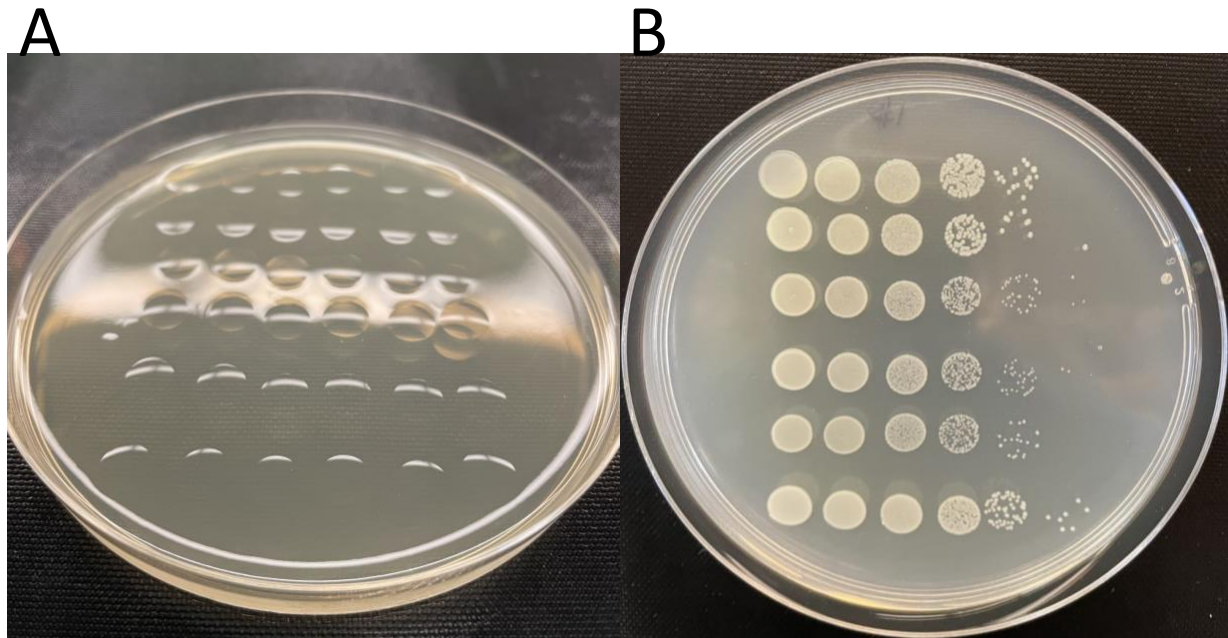
Fig. 4 Visual representation of the 6x6 drop plate method on an agar plate
The 6x6 drop plate method as seen on an agar plate. A) 7 µL of sample from the last 6 columns used on a 96-well plate were pipetted onto an agar plate in a series of six replicates to create a 6x6 grid. The spots were allowed to dry out for 20 minutes before incubated at 25ºC. B) The growth after 24 hours at 25ºC can be seen. A column was selected for colony counting. A column was selected where about 50-200 total colonies could be counted accurately. Using the dilution, the colony counts were then converted to CFU/mL for quantification.

Stationary Phase Survival Assay

Three milliliter LB cultures of *Salmonella* 14028s and STM3615::Cam were grown overnight at 37ºC shaking at 250 rpm. The OD_{600} of the overnight cultures was taken, and three 50 mL samples within 250ml beveled flasks of each strain were diluted to 0.1 OD_{600} as a 0 hour time point. The 0 hour cultures were measured for OD_{600}, and a sample was plated on LB plates using the 6x6 drop plate method described above. The 3 replicates were allowed to grow for 72 hours with OD_{600} and CFU counts taken at 6, 24, 48, and 72 hours to determine both bacterial density and viable counts.

Phase-Contrast Microscopy

Bacteria were grown overnight in M63 media containing amino acids. The M63 media contained 0.5x M63 salts (21 mM dibasic potassium phosphate, 11 mM monobasic potassium phosphate and 4.4 mM ammonium sulfate final concentration), 1x Corning® MEM essential amino acid solution, 1x Corning® MEM nonessential amino acid solution, 0.23% glycerol, 2 mM $MgCl_2$, 1 mM NaCl, and 10 µM $FeCl_3$[38]. The next day, a 0.75mm acrylamide gel pouring apparatus was filled with a solution of 1% agarose in 0.5x M63 salts and allowed to solidify. Overnight bacterial cultures were resuspended at a dilution of 1:100 in M63 media containing amino acids and grown for 2 hours at 37°C with shaking. Four discs of agarose were prepared using the large end of a 200 µL pipette tip and placed in a 2x2 grid on a glass slide. One milliliter of the 2 hour bacterial culture was removed, pelleted by centrifugation, and resuspended in 250 µL of the supernatant. One microliter of this resuspension was applied to an agarose disc and covered with a glass cover slip. These slides were imaged on a Nikon TiE microscope using a 100x oil objective. Bacterial size was quantified using the MicrobeJ ImageJ plug-in[39].

Complementation of STM3615

The coding sequence for STM3615 was cloned from the 14028s genome by PCR using the primers 3615Comp RBS F and 3615Comp R. This PCR fragment was initially cloned into the vector pTopo (Invitrogen) to generate pTopo-3615RBS, then removed by restriction enzyme digestion by the *EcoRI* and *HindIII* found within the designed primers and inserted into the expression vector pMMB67EH (pMMBA) (Fig. 5). When necessary, the STM3615 gene was induced by the addition of 1mm IPTG to the growth media.
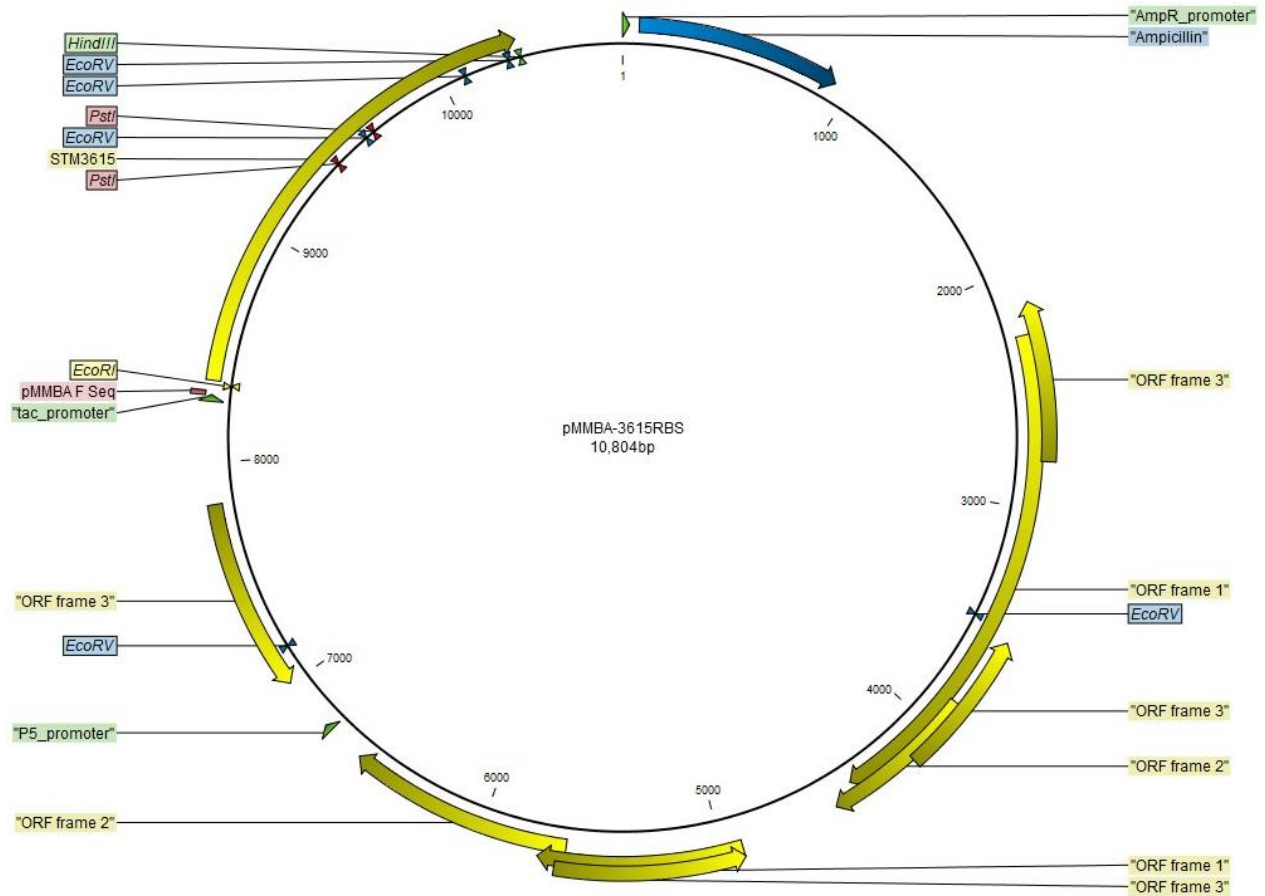
Fig. 5 pMMBA-3615RBS vector map
The pMMBA-3615RBS vector was used to complement the STM3615 deletion mutant. The base
vector is pMMBA with the full length STM3615 protein included. The vector contains the *bla*
gene which confers ampicillin resistance. The *tac* promotor, pTac, is used to express the
STM3615 gene in the presence of IPTG.

STM3615$_{\Delta peri}$ Mutant Construction

To generate the genomic periplasmic deletion of STM3615, the first step was to remove

the periplasmic domain from an STM3615 gene. Primers were designed containing an *NheI*

restriction site (3615 noPeri Fwd/Rvs [*NheI*]) that would delete the periplasmic domain upon

PCR of the entire pTopo-3615RBS vector and relegation at the newly generated *NheI* site. This

PCR was conducted, the resulting PCR fragment was digested with *NheI*, and it was ligated and

transformed into DH5α cells. This plasmid was then sequenced to confirm the appropriate periplasmic deletion and that there were no other mutations within the gene.

To prepare a PCR fragment for Lambda RED insertion, we would need to include both the STM3615$_{\Delta peri}$ coding region and a kanamycin resistance marker. The kanamycin resistance cassette from pKD4 was cloned into the pUC19 vector using primers designed to use the restriction sites *SalI* and *HindIII* (pUC19 Kan Fwd/Rvs [*SalI/HindIII*]). The resulting vector (pUCK) had the STM3615$_{\Delta peri}$ coding region inserted into it using a second set of primers (3615 pBAD Comp Fwd [*EcoRI*] & 3615SDM Int 3' Rvs [*SalI*]) and the restriction sites *EcoRI* and *SalI* (Fig. 6).
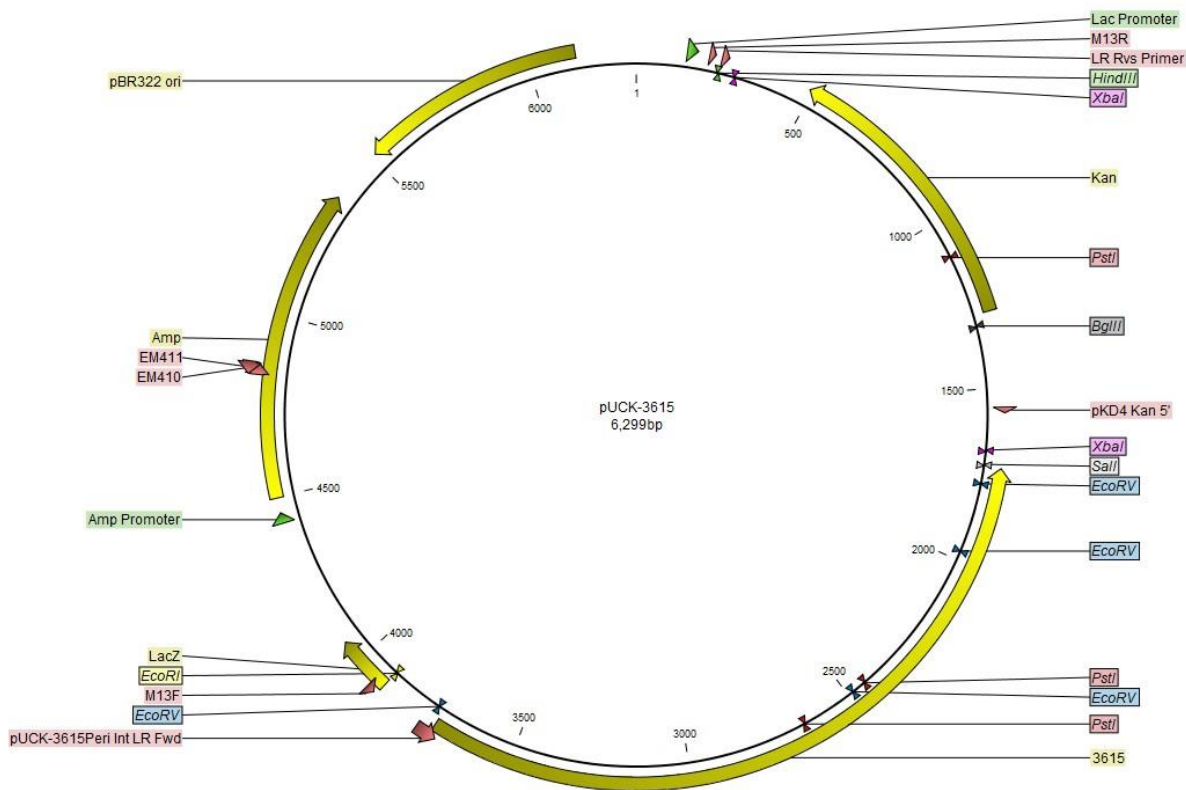
Fig. 6 pUCK-3615 vector map
The pUCK-3615 vector was used to replace the full length WT STM3615 gene with the STM3615$_{\Delta peri}$ coding sequence and the kanamycin resistance marker using Lambda RED recombination. The base vector is pUC19 with an added kanamycin resistance cassette from pKD4 and the STM3615$_{\Delta peri}$ coding sequence The vector contains the *bla* gene which confers ampicillin resistance.

The periplasmic deletion was then integrated into the genome using Lambda RED. Primers were designed to amplify the kanamycin resistance cassette and the STM3615$_{\Delta peri}$ coding sequence (Appendix C)[40]. In order to be amplified together, one primer had upstream homology for the STM3615$_{\Delta peri}$ coding sequence along with a complementary sequence overhang with the full length STM3615 gene, and the other primer had downstream homology for the kanamycin resistance marker as well as a complementary sequence overhang with the full length STM3615 gene (Fig. 7). Once the PCR product was confirmed, it was combined with pKD46-containing *S.* Typhimurium 14028swhose LR machinery allowed the recombination of the STM3615 gene with the STM3615$_{\Delta peri}$ coding sequence and kanamycin resistance marker. To get a purified Lambda Red (LR) PCR fragment, a mixture of 12.5 µL of GoTaq Master Mix, 10 µL of DNAse free H$_2$O, 1 µL of the forward LR KO primer, 1 µL of the reverse LR KO primer, and 0.5 µL of pUCK-3615$_{\Delta peri}$ template was combined. The thermocycler program was split into two parts. The first part consisted of 5 cycles with a 95ºC denaturation step for 30 seconds, a 45ºC annealing step for 30 seconds, and a 72ºC extension step for 2 minutes. The second part consisted of 30 cycles with a 95ºC denaturation step for 30 seconds, a 72ºC annealing step for 30 seconds, and a 72ºC extension step for 2 minutes. The PCR products were run out on a 1% agarose gel to confirm presence of the fragment. The fragment was extracted using the IBI Scientific™ Gel Extraction Kit and eluted with DNAse free H$_2$O.
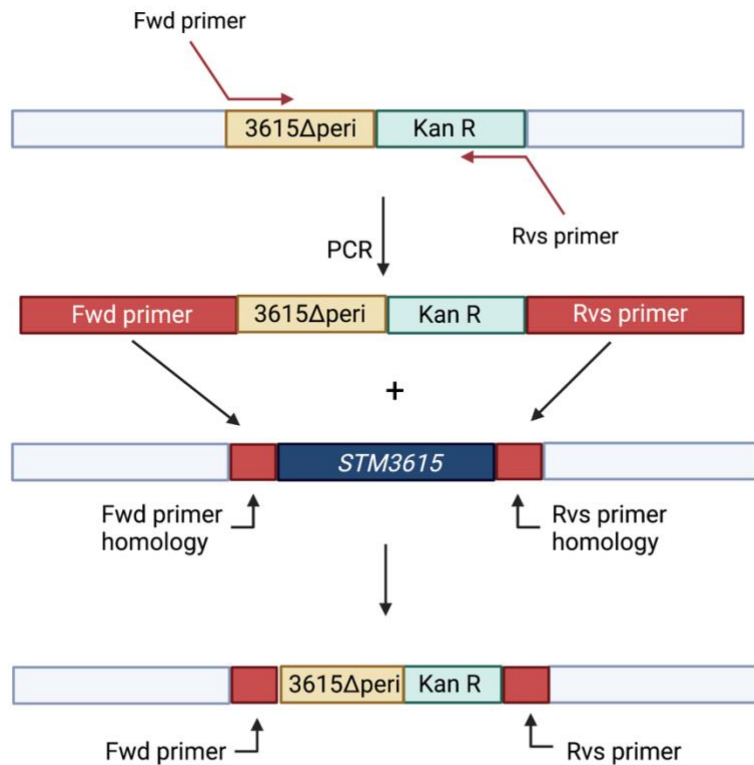
Fig. 7 Lambda RED recombination
Primers were created that had upstream and downstream homology overhangs with the target gene. These primers were used to produce a PCR product. This PCR product was then combined with pKD46. The LR machinery in pKD46 was induced, and recombination was possible with the overhang homology of the target genes, thus inserting the Kan/Cam resistance marker in place of the target gene. Figure created with Biorender.com

For *Salmonella* mutagenesis, pKD46-containing *S*. Typhimurium 14028s (Appendix B) was grown up from a freezer stock in 2 mL of LB + Amp^{100} at 30ºC shaking at 250 rpm. The overnight pKD46 culture was diluted 1:50 into new LB + Amp^{100} and grown for 2 hours at 30ºC shaking at 250 rpm. The LR machinery in pKD46 was induced by adding 0.2% arabinose and grown for another hour. After the culture was induced, it was prepared for electrocompetent cells. 500 µL of the induced pKD46 culture was transferred to a 1.5 mL tube and centrifuged for 2 minutes at 15,000 rpm, then washed and centrifuged three times with cold water for 2 minutes

at 15,000 rpm. After the third wash, the culture was resuspended with enough cold water to fulfill a volume of 100 µL per reaction and extra for a control plate. 97.5 µL of electrocompetent cells were added to a 1.5 mL tube and mixed with 2.5 µL of purified LR PCR product. The mixture was transferred to an electroporation cuvette and shocked at 1.8 kV. 1 mL of SOC medium was added to both the electroporation cuvette culture and the electrocompetent pKD46 control culture, mixed, and transferred to a 5 mL tube to incubate at 37ºC shaking at 250 rpm for 2 hours. The cultures were then plated onto LB plates with Kan[100] and incubated overnight at 37ºC.

Resistant colonies were grown overnight in LB broth containing kanamycin and amplified in a thermocycler to confirm gene deletion. Fifty microliters of an overnight culture was centrifuged within a PCR tube, the LB supernatant was removed, and the pellet was resuspended in 50 µL of DNAse-free water. This sample was boiled for 10 min in a thermocycler, then centrifuged for 5 min to pellet any cellular debris. 1 µL of the resulting supernatant was used as the template DNA for a PCR with 5 µL of GoTaq 2x Master Mix, 0.5 µL of forward KO confirmation primer, 0.5 µL of reverse KO confirmation primer, and 3 µL of DNAse free H_2O. The thermocycler went for 40 cycles with each cycle consisting of a 98ºC denaturation step for 30 seconds, a 57ºC annealing step for 30 seconds, and a 72ºC extension step for 3 minutes and 30 seconds. The PCR fragments were then run out on a 1% agarose gel to confirm gene deletion based on a size comparison to the wild type sequence.

In order to ensure a clean strain, the mutation was transferred back to *Salmonella* Typhimurium strain 14028s using a modified P22 phage[41]. A 2 mL LB + Kan[100] culture of *STM3615[Δperi]*::Kan was grown overnight at 37ºC shaking at 250 rpm. The next day in a 5 mL tube, 1 mL of LB, 1.5 µL of P22-HTInt phage from *Salmonella* Typhimurium strain 14028s, and

500 µL of the overnight culture were mixed and grown overnight at 37ºC shaking at 250 rpm. A

2 mL LB culture of *Salmonella* Typhimurium strain 14028s was also grown overnight at 37ºC

shaking at 250 rpm to serve as a phage recipient. After incubation, 1 mL of the mixed culture

was transferred to a 1.5 mL tube and centrifuged for 2 minutes at 15,000 rpm. 900 µL of the

supernatant was transferred to a new 1.5 mL tube, mixed with 100 µL of chloroform to kill any

remaining bacteria, and allowed to sit for 5 minutes. The mixture was then vortexed and

centrifuged for 2 minutes at 15,000 rpm to separate the layers. The aqueous supernatant,

containing the clean P22 phage, was transferred to a glass vial for storage.

Then, in a 5 mL tube, 2 µL of the clean P22 phage with the donor mutation was added to

1 mL of LB. In two more 5 mL tubes, 150 µL of overnight *Salmonella* Typhimurium recipient

culture of each strain was added. One tube of the pair received 150 µL of LB to act as a control.

The other tube received 150 µL of the diluted P22 stock. Tubes containing the *Salmonella* + LB

control, diluted P22 stock, and *Salmonella* + P22 stock were incubated for 2 hours at 37ºC

shaking at 250 rpm. The cultures were then plated on LB + Kan^{100} plates overnight at 37ºC.

Resistant colonies were then streaked onto green plates to separate the phage. A white colony

from the green plates was then streaked onto a new green plate to ensure the phage was gone.

From the second green plate, a white colony was used to inoculate LB + Kan^{100} for 24 hours at

37ºC shaking at 250 rpm.

A sample from the overnight culture was boiled in water at 98ºC for 10 minutes and used

as template DNA. 1 µL of the template DNA was combined with 5 µL of GoTaq 2x Master Mix,

0.5 µL of the reverse primer, 0.5 µL of the forward primer and 3 µL of DNAse free H$_2$O. The

thermocycler went for 40 cycles with each cycle consisting of a 98ºC denaturation step for 30

seconds, a 55ºC annealing step for 30 seconds, and a 72ºC extension step for 30 seconds. To

check for the presence of lysogenic phage, a pipette tip was dipped into the P22 strain H5 phage and dragged along the length of a green plate. 1 µL of *Salmonella* Typhimurium strain 14028 with gene deletion was added to the green plate and dragged from one side of the plate through the H5 line to the other side of the plate. The green plate was then incubated at overnight at 37ºC. Cultures that changed to a blue color upon encountering the H5 phage line are free of lysogenic phage.

<p style="text-align:center">A22 Qualitative Survival Assay</p>

During concentration testing for A22, it was determined that LB plates with 2 µg/mL of A22 at 25ºC was sufficient to see a clear difference in survival between *Salmonella* 14028s and STM3615::Cam. To identify transposon mutants that showed a reversion to the WT ability to survive A22, *Salmonella* 14028s, STM3615::Cam, and all 41 of the transposon mutants were inoculated in 1 mL of LB and grown overnight at 37ºC, shaking at 250 rpm. These samples were diluted similarly to the 6x6 drop plate method for a 10-fold serial dilution for each bacterial sample. A single replicate of 7 µL spots from the last six columns was then plated on both LB plates and LB + A22 plates and incubated at 25ºC for two days to qualify bacterial growth of all the samples. All bacterial samples were replicated at least twice. A scoring system was made to qualify the bacterial growth that went from no growth, or a growth score from 1-6. No growth meant that there was no visible bacterial growth where the 7 µL spots were pipetted. 1 through 6 indicate the maximum number of 7 µL spots where bacterial growth was seen. A score of 6 was the most growth as a diluted bacterial sample of 10^{-11} still exhibited growth. Typically, *Salmonella* 14028s scored a 5 for both the LB and LB + A22 plates while STM3615::Cam scored a 5 for the LB plates and a 2 for the LB + A22 plates. Some transposon mutants exhibited no change in growth between the LB and LB + A22 plates, but they had lower survival levels

over all on the LB plates, so they were excluded. The transposon mutants with the growth closest

to 14028s were tested again.

Bioinformatic Analysis of STM3615

To determine the domain organization of STM3615, bioinformatic analysis with three

different tools was used. SMART is a tool that can identify more than 500 known domain

families from the amino acid sequence of a protein[42,43]. The amino acid sequence for STM3615

was put into the SMART program for analysis, and the presence of five domains was discovered:

two transmembrane domains, a periplasmic domain situated between them, a DGC GGDEF

domain, and an PDE EAL domain. NCBI's Conserved Domain Database (CDD) that uses both

amino acid and nucleotide sequences to compare to known domain sequences to predict the

domain structure of proteins was also used[44]. By inserting STM3615's amino acid sequence, the

presence of the same five domains was discovered: two transmembrane domains, a periplasmic

domain situated between them, a DGC GGDEF domain, and an PDE EAL domain. To

understand the potential function of the periplasmic domain of STM3615, Protein

Homology/Analogy Recognition Engine (PHYRE) was employed. PHYRE is a tool that

compares amino acid sequences to known crystallized proteins to match nearest homologs[45]. The

periplasmic domain amino acid sequence was entered into the program, and the predicted

structure and its closest homologs were shown.

Free Periplasmic Domain Construction

To express only the STM3615 periplasmic domain within the periplasm, a set of primers

was designed to insert this fragment into the expression vector pBAD24 (3615Peri-PagC

Fwd/Rvs [*EcoRI/HindIII*]). In addition to an *EcoRI* restriction site and complementary sequence

to the beginning of the 3615 periplasmic domain (just downstream of the first transmembrane

domain), it also contains the start codon and signal peptide-coding sequence from the periplasmic protein PagC[46]. This *pagC* signal peptide sequence will enable the free STM3615 periplasmic to be exported to the periplasm through the Sec secretory pathway[22]. The reverse primer contains a *HindIII* site and sequence complementary to the 3' end of the STM3615 periplasmic domain just upstream of the final transmembrane domain, which should give us a complete, secretable periplasmic domain. The periplasmic domain PCR fragment was generated from *S.* Typhimurium genomic DNA and cloned into the pBAD24 expression vector (Fig. 8). After sequencing to confirm the integrity of the cloned product, this expression vector was electroporated into the ΔSTM3615 mutant and selected on LB+Amp[100] plates. When expression was desired, the vector was induced using 0.2% arabinose in the growth media.
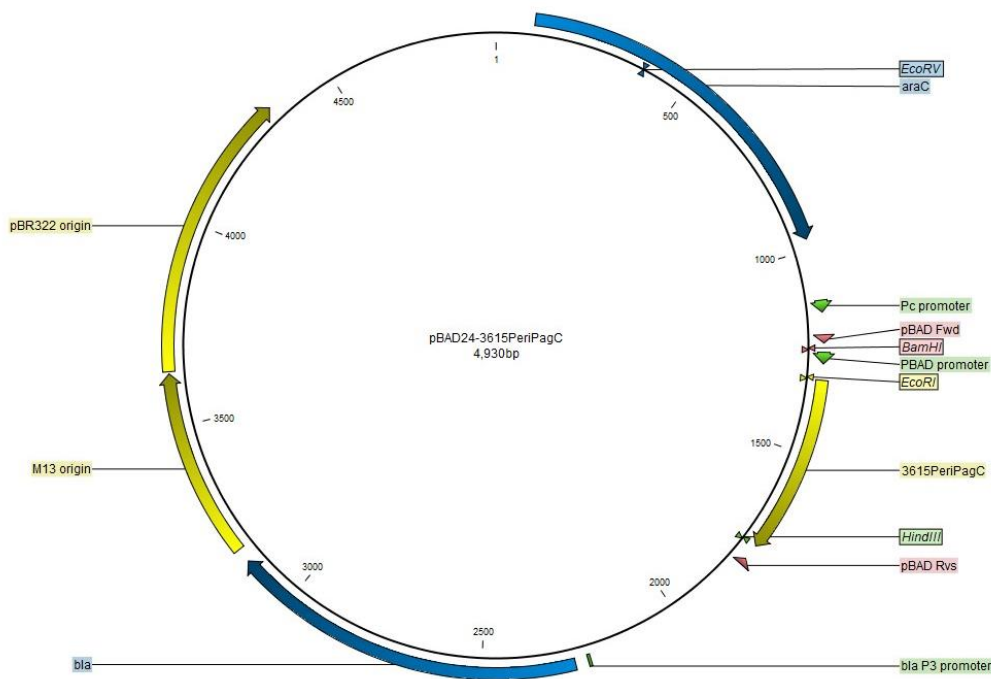
Fig. 8 pBAD24-3615PeriPagC vector map
The pBAD24-3615PeriPagC vector was used to express only the STM3615 periplasmic domain within the periplasm. The parent vector is pBAD24. The vector contains the *bla* gene which confers ampicillin resistance. The periplasmic domain coding sequence starts just downstream of the first transmembrane domain and ends just upstream of the second transmembrane domain. To make sure that the periplasmic domain is secreted to the periplasm, a signal peptide sequence from the periplasmic protein PagC was included.

Transposon Mutagenesis Assay

Both the *Salmonella* mutant STM3615::Cam and mariner transposon vector pBT20

within the conjugation strain SM10 (Appendix A) were plated from frozen stocks into 150 μL of

LB media atop either an LB + Cam^{34} or LB + Gent^{30} agar plate respectively and allowed to

incubate at 37ºC overnight. Bacteria was scraped from plates into LB broth and the optical

density of the bacteria was determined using a spectrometer. STM3615::Cam was diluted to 20

OD, and SM10/pBT20 was diluted to 40 OD. Diluted cells of STM3615::Cam and SM10/pBT20

were combined, ten 50 μL spots of the mixture were pipetted onto 2 LB plates and allowed to

incubate at 37ºC for 2 hours. Two 50 μL spots of the separate diluted STM3615::Cam and

pBT20 samples was also pipetted onto a LB plate and allowed to incubate at 37ºC for 2 hours to

serve as controls. After incubation, bacterial spots were scraped into LB broth and plated to

green plates + Cam^{34}/Gent^{30} alongside the control spots (Fig. 9). All plates were incubated at

37ºC for a maximum of 4 days to allow for growth of white colonies. White colonies (revertants

from the STM3615 deletion mutant phenotype) were transferred to LB + Cam^{34}/Gent^{30} to grow

overnight for preservation and PCR.
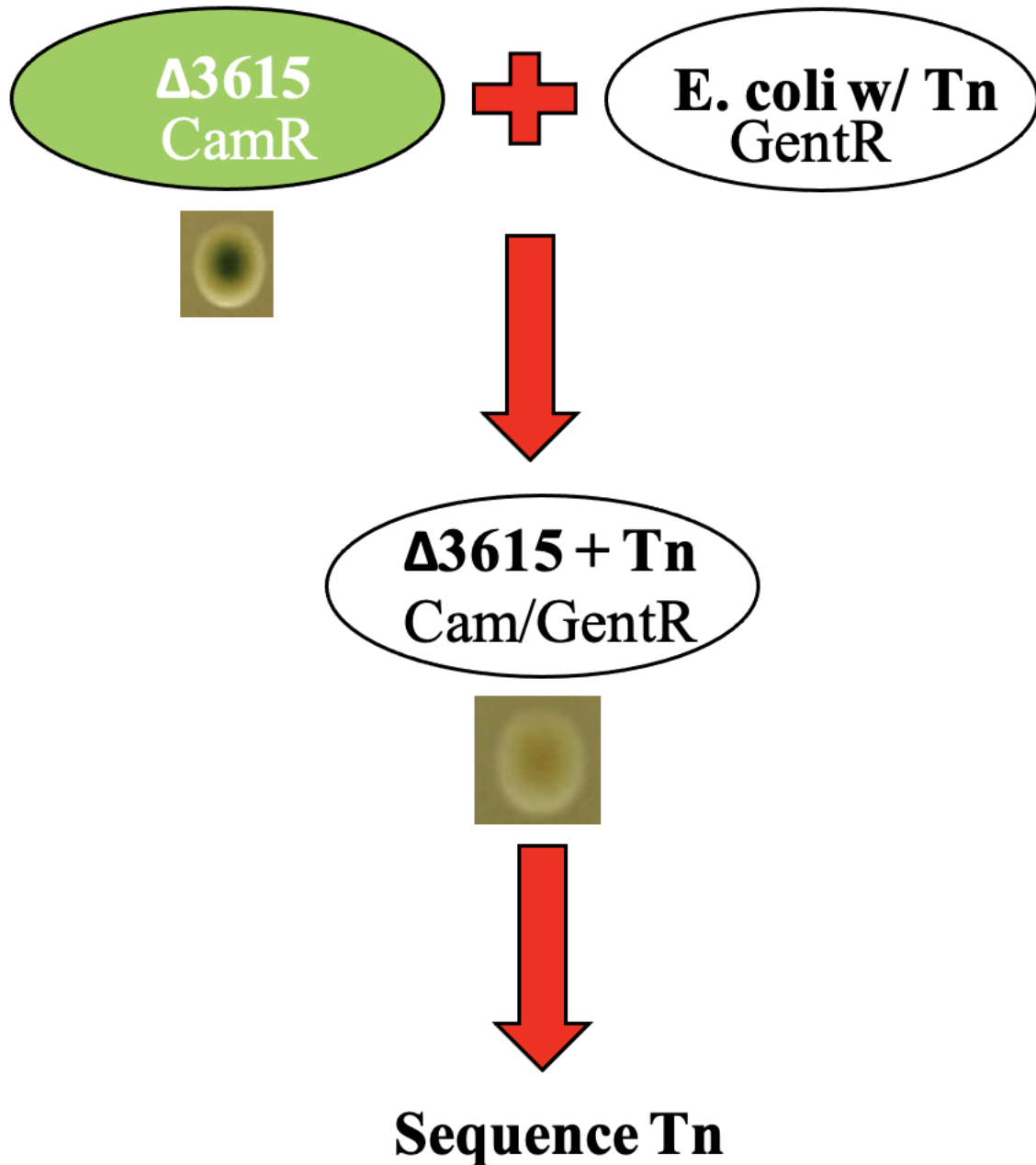
Fig. 9 Transposon mutagenesis schematic
The ΔSTM3615 mutant, which is chloramphenicol resistant, and SM10-λpir containing pBT20, which is gentamicin resistant, were mixed together to conjugate. This conjugation mixture was plated onto green plates containing Cam^{34}/Gent^{30}. Colonies were chosen if they had a WT white phenotype unlike the ΔSTM3615 mutant's blue/green center phenotype.

To determine the location of the transposon insertion within my white colonies, 50 µL of

overnight culture was transferred to a PCR tube. The sample was centrifuged for 5 minutes at

15,000 rpm, the LB supernatant was removed and replaced with 50 µL of DNAse free H_2O and vortexed to resuspend the pellet. In a thermocycler, the sample underwent the BOIL protocol which consisted of one 10 minute cycle at 98ºC. The sample was then centrifuged for 5 minutes at 15,000 rpm, and the supernatant used as the DNA template for PCR. The template underwent rounds of PCR according to the protocol by Kulasekara[47]. For the first round of PCR, 1.0 µL of template DNA was combined with 8.7 µL of DNAse free H_2O, 2.0 µL of Rnd1-ARB, 0.8 µL of Rnd1-TnM20 (Appendix C), and 12.5 µL of GoTaq 2x Master Mix. The first round thermocycler program consisted of 2 parts. The first part consisted of 15 cycles of a 94ºC denaturation step for 30 seconds, a 49ºC annealing steps for 30 seconds that reduced in temperature by 1ºC every cycle, and a 72ºC extension step for 3 minutes. After 15 cycles, the second part consisted of 20 cycles of a 94ºC denaturation step for 30 seconds, a 60ºC annealing steps for 30 seconds, and a 72ºC extension step for 3 minutes. The Rnd1-TnM20 primer is a transposon-specific primer that lays down the furthest into the transposon. The Rnd1-ARB is a series of four arbitrary primers that can be used separately or as a mixture that have a variety of binding-sites in the chromosome. These two primers and the DNA between them make up the Rnd1 PCR product to be used in the second round of PCR (Fig. 10). 2.0 µL of the first round PCR product was then added to 21.4 µL of DNAse free H_2O, 0.8 µL of Rnd2-ARB, 0.8 µL of Rnd2-TnM20, and 25.0 µL of GoTaq 2x Master Mix. The second round PCR program consisted of 30 cycles of a 94ºC denaturation step for 30 seconds, a 60ºC annealing steps for 30 seconds, and a 72ºC extension step for 2 minutes. The extension step was followed by a 72ºC step for 5 minutes. The Rnd2-TnM20 is a transposon-specific primer that overlaps the Rnd1-TnM20, allowing Rnd2-TnM20 to sit on the Rnd1 PCR product. The Rnd2-ARB is an arbitrary primer that hybridizes into the Rnd1-ARB primers. Together, the Rnd2 PCR product is made (Fig. 10). The PCR fragments

were then cleaned using the IBI Scientific™ PCR DNA Fragments Extraction Kit. 10 µL of

cleaned PCR product was added to 4 µL of DNAse free H_2O and 1 µL of Seq-TnM20 and sent

out for sequencing. Returned sequencing was entered into the NCBI's BLAST program where it

was compared against the *S*. Typhimurium 14028s genomic DNA to determine the site of the

transposon insertion[48].
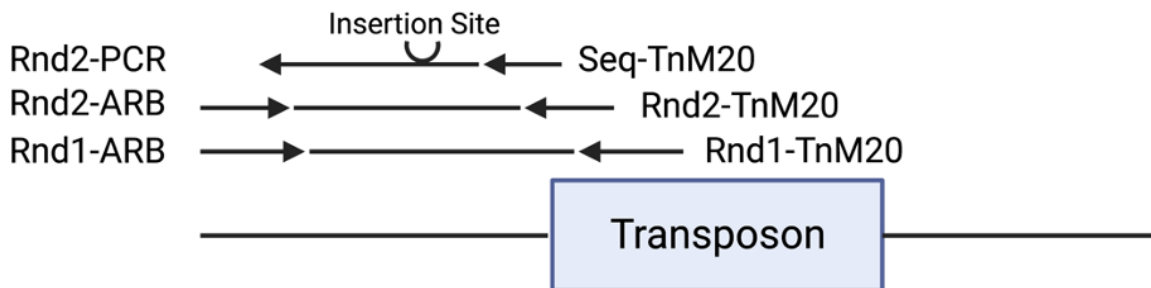
Fig. 10 Arbitrary PCR schematic
The first round of ARB PCR lays down the Rnd1-TnM20 and Rnd1-ARB primers onto the target
DNA. The second round of ARB PCR lays down the Rnd2-TnM20 and Rnd2-ARB primers onto
the Rnd1-PCR product. The Rnd2-PCR product is sequenced using the Seq-TnM20 primer that
lays down on the transposon junction to identify the transposon insertion site. Figure created
with BioRender.com

CHAPTER 3. RESULTS

ΔSTM3615 Mutant Displays Phenotype on Phage Killing Plates

Deletions of each cyclic-di-GMP-modulating enzyme in *Salmonella* Typhimurium were

generated during previous studies[38]. Part of this mutant construction involved transducing these

mutations through the use of a modified P22 phage, which necessitated clearing the remaining

phage through the use of a phage killing plate to monitor for cell death ("green phage plates")[41].

The glucose present in the agar acidifies their cytoplasm, so when the *Salmonella* lyse from

phage infection, it causes the bacterial colony to appear blue/green (Fig. 11A). Interestingly,

when the mutant for the PDE STM3615 was plated onto a green phage plate, it displayed a

similar green colony phenotype without phage infection as compared to the white WT colony

(Fig. 11B). The ΔSTM3615 mutant continued to have this phenotype even when repeatedly

inoculated onto new plates, indicating it was not a case of phage infection.
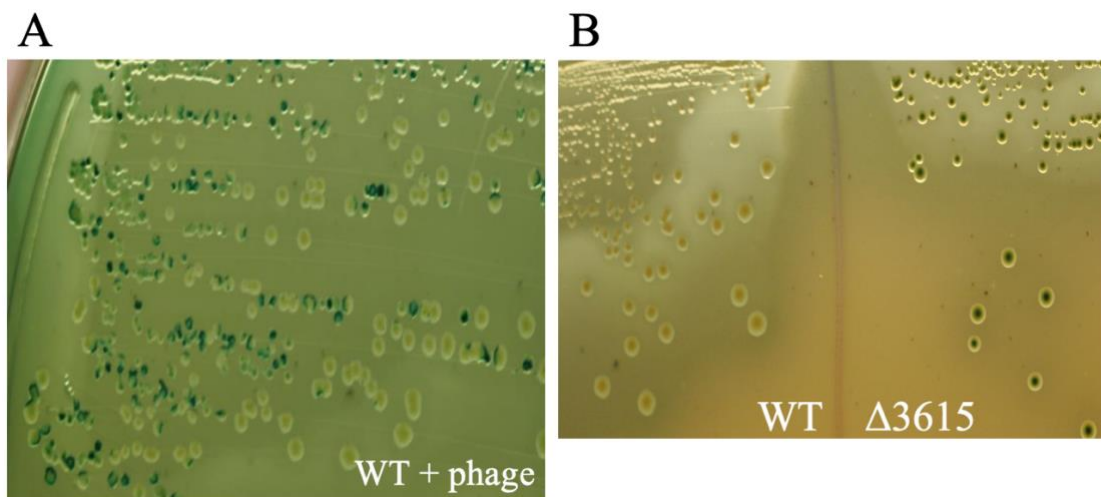
Fig. 11 WT and ΔSTM3615 phenotypes on green agar plates
A) Bacterial colonies of WT *Salmonella* Typhimurium infected with P22 phage can be seen on a green phage plate. The colonies that are green/blue are indicative of phage as the cytoplasm of the bacteria acidifies from glucose in the medium is released after cell lysis. The white colonies are not infected with phage, resulting in an intact cell and no resulting dye color change. B) On the left, ΔSTM3615 mutant colonies uninfected by phage can be seen to exhibit a blue/green circle in the middle, resembling dead cells in A. On the right, WT *Salmonella* Typhimurium colonies uninfected by phage have a typical white appearance.

The ΔSTM3615 Mutant and WT Have No Difference in Growth

We hypothesized that the reason for cell death on the green phage plates was due to an inability of the ΔSTM3615 mutant to survive the transition to stationary phase. I wanted to try and replicate this data in liquid culture by monitoring stationary phase survival. Overnight cultures of *Salmonella* 14028s and the ΔSTM3615 mutant were diluted to 0.1 OD_{600} in LB. The OD_{600} and viable CFUs of the each culture was taken at the 0, 6, 24, 48, and 72 hour time points to determine both the bacterial cell density and the cell viability in the samples (Fig. 12). Neither assay appeared to indicated a difference between WT and the ΔSTM3615 mutant, although it may still be of further interest with a different experimental design.
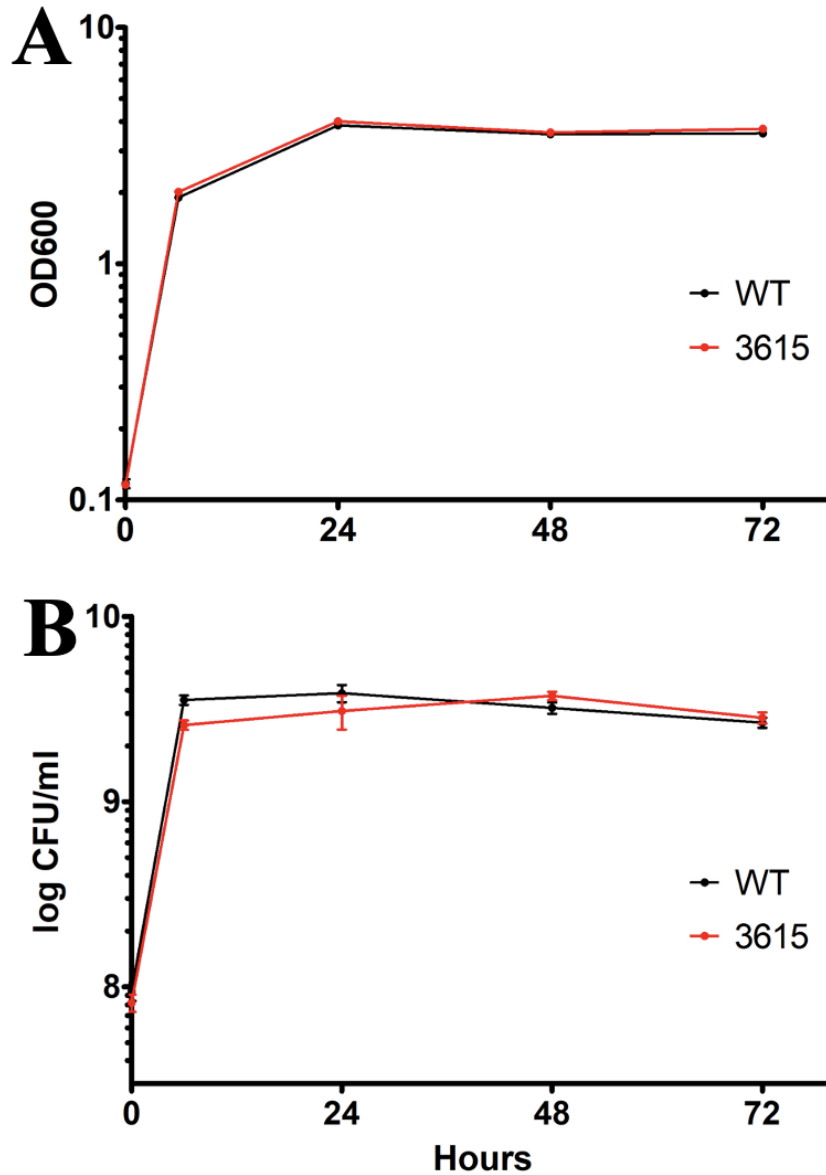
Fig. 12 WT and STM3615 OD_{600} and CFU/mL growth curve over 72 hours

Three mL LB cultures of *Salmonella* 14028s and ΔSTM3615 were grown overnight. The OD_{600} of the overnight cultures was taken and diluted to 0.1 OD_{600} in 50 mL LB samples in 250 mL beveled flasks. At the 0, 6, 24, 48, and 72 hour points, the A) OD_{600} of the three replicates was taken and the B) CFU/ml was determined by plating onto LB plates using the 6x6 drop-plate method. Results were analyzed using two-way ANOVA with a post-hoc Bonferroni test. The samples were found to not be statistically different.

ΔSTM3615 Mutant Is Shorter than WT

As the colony morphology of the ΔSTM3615 mutant was different compared to the WT, the two strains' cell morphology were examined under phase-contrast microscopy. Compared to the WT *Salmonella* Typhimurium, the ΔSTM3615 mutant was shorter (Fig. 13A-B). To determine that the deletion of the STM3615 gene was the cause, the ΔSTM3615 mutant was complemented via an inducible plasmid vector. Not only was the WT length phenotype was restored, but overexpression of STM3615 increased the length of the bacteria beyond the WT phenotype (Fig. 13C). The quantification for these three strains showed that the length was significantly different (Fig. 17).
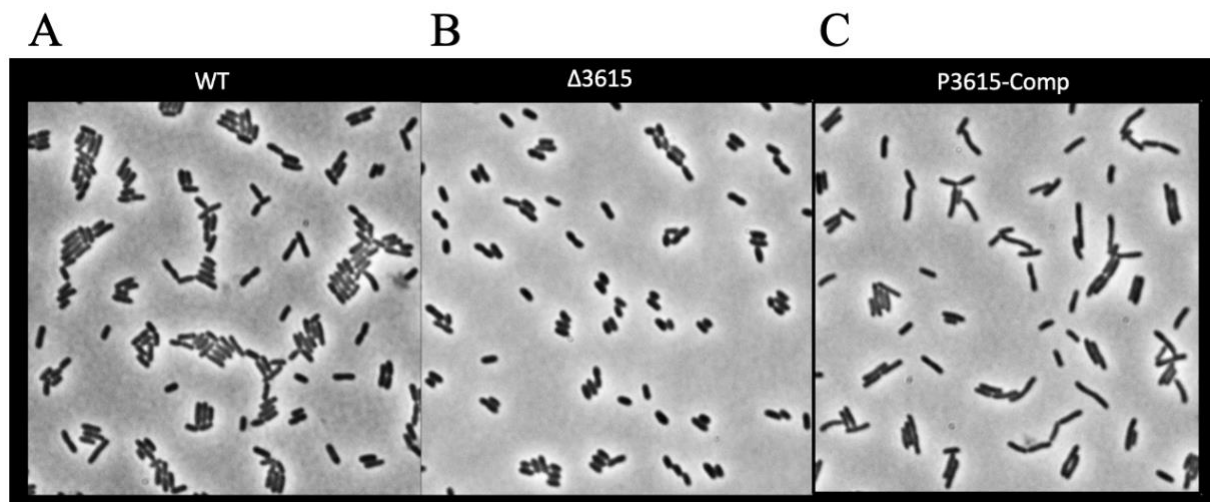
Fig. 13 Phase-contrast microscopy of *Salmonella*
A) WT *Salmonella* Typhimurium, B) ΔSTM3615 mutant, and C) STM3615-overexpressing cells can be seen under the phase-contrast microscope. The ΔSTM3615 mutant displays a shorter, wider bacterium shape, while over-expression of the STM3615 gene results in bacteria longer than wild type.

Bioinformatic Analysis of STM3615 Reveals an Inner Membrane Phosphodiesterase with Multiple Domains

To better examine STM3615, its protein sequence was analyzed through several bioinformatic techniques. Simple Modular Architecture Research Tool (SMART) domain analysis (Fig. 14A) and a domain search through the NCBI's Conserved Domains Database (CDD) (Fig. 14B) identified two transmembrane domains, a periplasmic domain between them, a DGC GGDEF domain, and a PDE EAL domain[42–44]. Analysis of the protein sequence suggests that the DGC domain is degenerate due to the alternative active side residues present (SGYDF), while the PDE domain contains all the necessary amino acids for catalysis[49,50]. Further comparison with similar domain architectures in other proteins suggests the presence of a HAMP domain (Fig. 2), a small domain that serves to transmit protein conformational changes from one side of a membrane to the other[31].
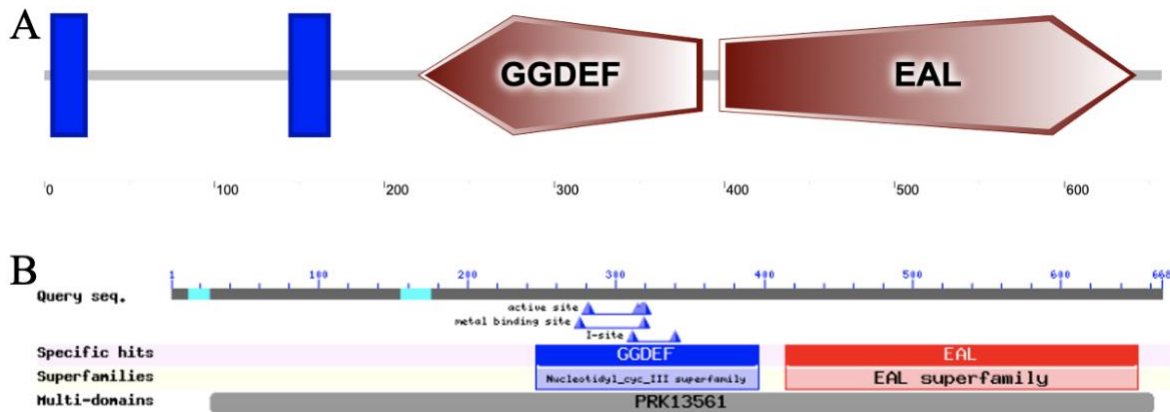
Fig. 14 SMART and CDD analysis of STM3615
A) The SMART and B) CDD analysis gave the domain make-up of STM3615 complete with its two transmembrane domains (blue bars in A), the periplasmic domain found between them, a GGDEF domain, and an EAL domain. Sequence analysis of the GGDEF domain found that the active site was degenerate from the consensus (SGYDF), meaning it is likely inactive.

A22 Antibiotic Stunts ΔSTM3615 Mutant Growth, Dependent on the Periplasmic Domain but

Not Phosphodiesterase Activity

The antibiotic A22 is a MreB inhibitor used in bacterial cytoskeletal research that works

by reversibly binding to MreB's ATP-binding pocket[51]. This binding prevents MreB proteins

from polymerizing into filaments. A22 was originally found during a screening of inhibitors of

chromosome partitioning in *Escherichia coli*[52]. Because of MreB's association with cell

morphology and the ΔSTM3615 mutant's unique length phenotype, we wanted to observe if the

loss of MreB function impacted the ΔSTM3615 mutant more than the WT *Salmonella*

Typhimurium. Through concentration testing, it was determined that a concentration of 2 µg/mL

of A22 at an incubation temperature of 25ºC showed the best visual difference between the two

strains. LB plates with a concentration of 2 µg/mL of A22 were used to test the growth of the

two strains. Using the 10-fold 6x6 drop plate method, both strains were plated on LB and LB +

A22 plates and allowed to incubate at 25ºC for two days. While the WT showed a moderate

inhibition on the A22 plate compared to the LB plate, the ΔSTM3615 mutant exhibited a

dramatic reduction in survival (Fig. 15). For the ΔSTM3615 mutant to be particularly sensitive to

A22, it could suggest that STM3615 is involved in the replication of the cell, and when both

MreB and STM3615 are not functional, the cell cannot replicate to normal levels.

To further investigate the function of the various domains of STM3615, 2 additional

mutants were made at the STM3615 genetic locus. The first mutant, generated from a previous

study, was an active site mutation in the PDE domain that converted the catalytic EAL amino

acid residues to AAA (STM3615$_{AAA}$) that has been shown in both other PDEs and well as

STM3615 to remove the PDE activity from the protein (data not shown)[29,50]. The second

mutation was to remove the periplasmic domain from the protein, deleting this domain but

leaving the two transmembrane domains with a short connector (STM3615$_{\Delta peri}$). These strains were also subjected to A22 testing (Fig 15). While the PDE mutant exhibited survival similar to the WT strain, deletion of the periplasmic domain replicated the STM3615 full deletion mutant (Fig 15). This suggests that the periplasmic domain, rather than the c-di-GMP phosphodiesterase activity, is responsible for the bacterial morphology phenotype.
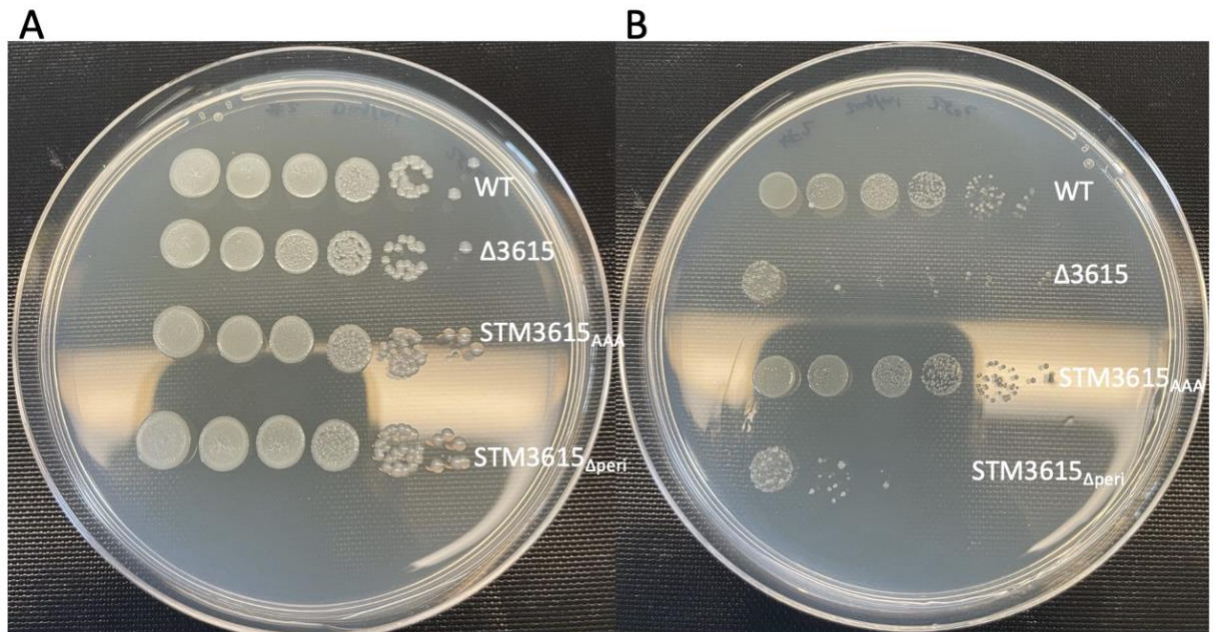
Fig. 15 ΔSTM3615 mutant without periplasmic domain has stunted growth compared to WT in presence of A22 antibiotic
A) WT, the ΔSTM3615 mutant, STM3615$_{AAA}$ mutant, and STM3615$_{\Delta peri}$ mutant grown according to the 6x6 drop plate method on LB plate. B) WT, the ΔSTM3615 mutant, STM3615$_{AAA}$ mutant, and STM3615$_{\Delta peri}$ mutant grown according to the 6x6 drop plate method on LB + A22^2 plate. The ΔSTM3615 mutant and the STM3615$_{\Delta peri}$ mutant exhibit less growth compared to the WT and the STM3615$_{AAA}$ mutant.

<u>STM3615 Periplasmic Domain is Responsible for Bacterial Size Differences</u>

While it appears from the A22 testing that the periplasmic domain of STM3615 is involved in the bacterial morphology phenotype, it was possible that deleting the periplasmic domain caused the full protein to misfold, making it look like the deletion strain. To further examine this phenotype, the STM3615 periplasmic domain was expressed as a free protein using

a signal peptide to export the protein to the periplasmic space (pFreePeri). Even though this

protein lacked the transmembrane domains and all cytoplasmic domains, it was sufficient to

lengthen the bacteria in the same way as the overexpressed full-length STM3615 protein (Fig.

16) and phosphodiesterase site-directed mutant (p3615$_{AAA}$ Fig. 16). Quantification of these

strains' length supports the phenotype (Fig. 17, 18).This again suggests that the presence or

absence of the periplasmic domain is the cause for the phenotypic differences related to the

STM3615 protein rather than the phosphodiesterase activity.
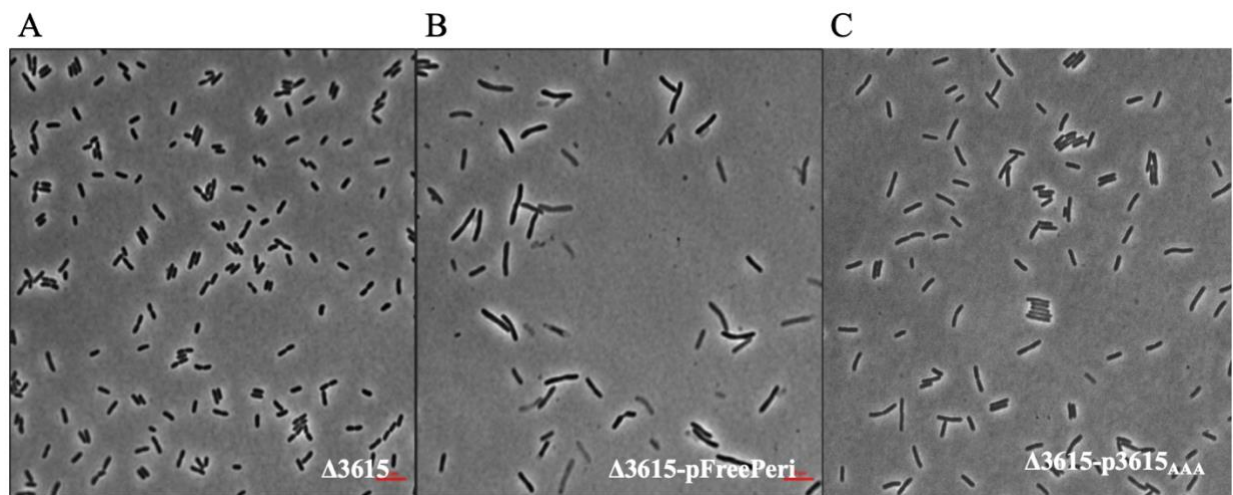
Fig. 16 Phase-contrast microscopy of the ΔSTM3615 mutant, the ΔSTM3615-p3615FreePeri
mutant, and the ΔSTM3615-p3615$_{AAA}$ mutant
A) The ΔSTM3615 mutant can be seen under a phase-contrast microscope. B) The ΔSTM3615-
pFreePeri mutant can be seen under a phase-contrast microscope. These cells are longer in length
compared to A. C) Overexpression of the STM3615$_{AAA}$ mutant can be seen under a phase-
contrast microscope. These cells are longer in length compared to A, but similar in length
compared to B. This suggests that presence of the periplasmic domain is required for the size
increase, rather than phosphodiesterase activity.
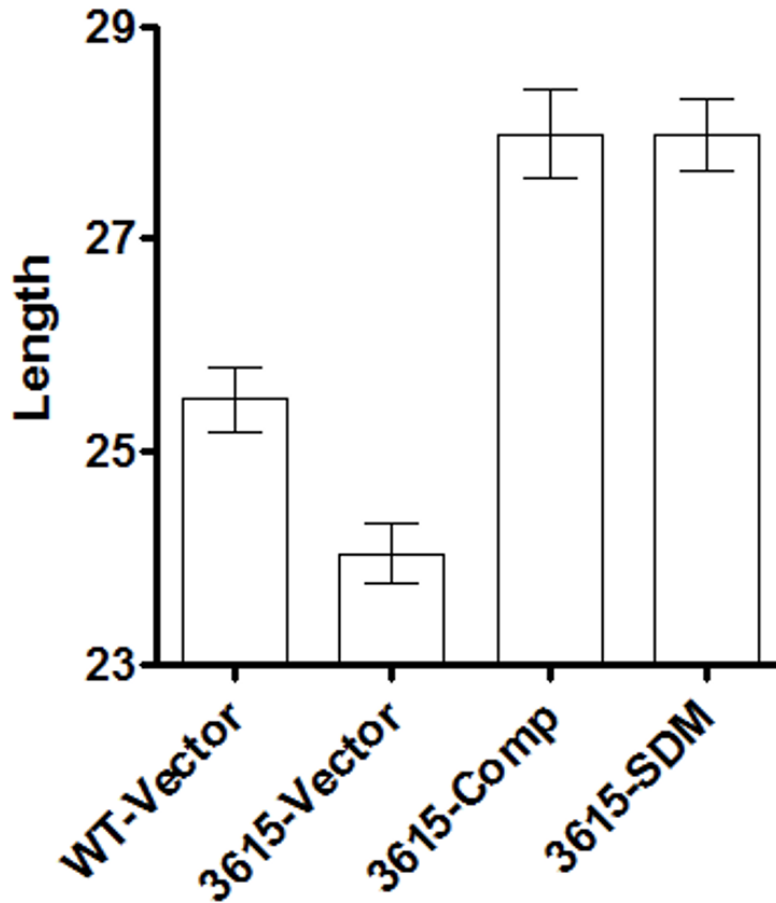
Fig. 17 Quantification of bacterial length of WT, the ΔSTM3615 mutant, STM3615-overexpressing cells, and the ΔSTM3615$_{AAA}$ mutant

The bacterial length of WT, the ΔSTM3615 mutant, STM3615-overexpressing cells, and the ΔSTM3615$_{AAA}$ mutant measured in pixels with 90 nm/pixel. The ΔSTM3615 mutant is shorter than its WT counterpart while upon overexpression of STM3615, the length increases past the WT. Without phosphodiesterase activity, the ΔSTM3615$_{AAA}$ mutant was comparable to the restoration of the full length STM3615 protein.
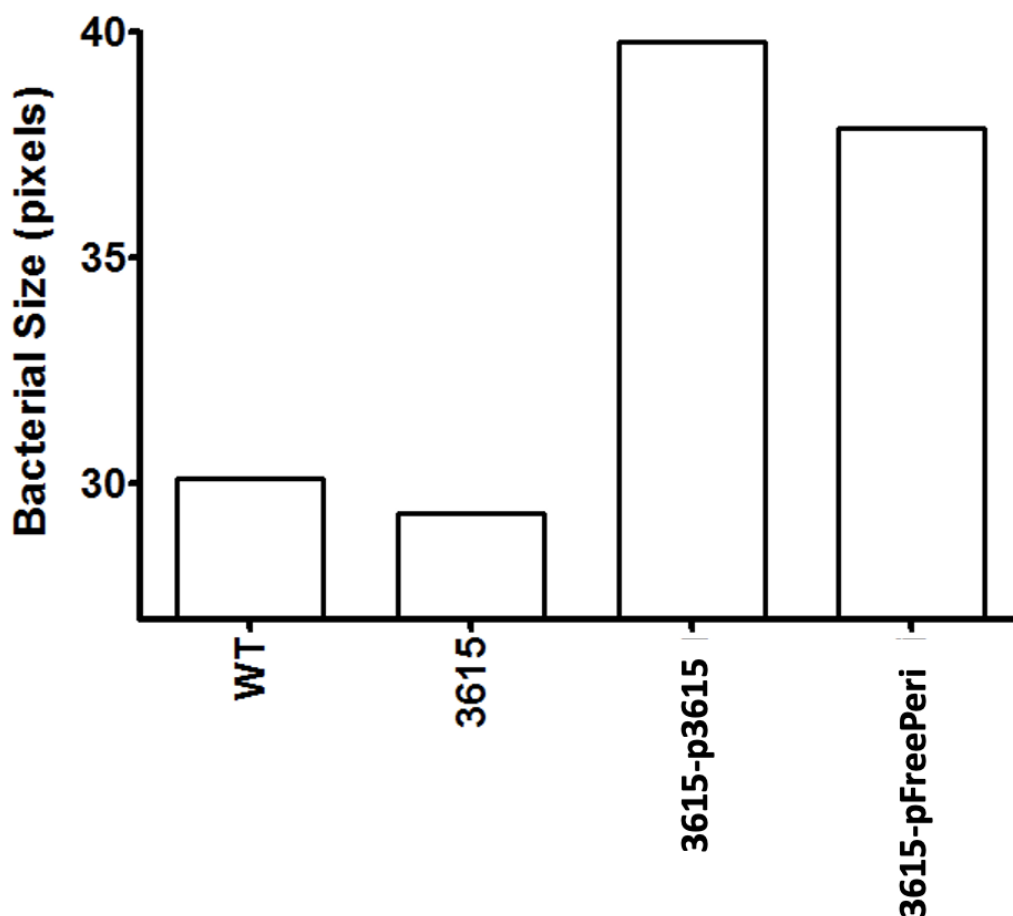
Fig. 18 Quantification of bacterial length of WT, the ΔSTM3615 mutant, STM3615-overexpressing cells, and STM3615-FreePeri overexpressing cells
The bacterial length of WT, the ΔSTM3615 mutant, STM3615-overexpressing cells, and STM3615-FreePeri overexpressing cells measured in pixels with 90 nm/pixel. The first three strains show the same effect as shown in Figure 17. The presence of just the STM3615 free periplasmic domain has a comparable length to STM3615-overexpressing cells and the ΔSTM3615$_{AAA}$ mutant, suggesting that the periplasmic domain is responsible for this phenotype.

<u>STM3615 Periplasmic Domain Has Most Similarity to LapD Periplasmic Domain</u>

To understand more about the potential function of the STM3615 periplasmic domain, I

employed the Protein Homology/Analogy Recognition Engine (PHYRE)[45]. PHYRE compares

your amino acid sequence to all the known crystallized proteins to identify its nearest homologs.

PHYRE aligns unknown sequences with known sequences, then, based on this alignment, a

structure for the unknown sequence is constructed based on the known structure. The closest

match to the STM3615 periplasmic domain was the periplasmic domain of a protein called LapD found in *Pseudomonas fluorescens* Pf0–1 (Fig. 19). LapD is a cyclic-di-GMP effector protein that has degenerate GGDEF and EAL domains, but it is still able to bind to cyclic-di-GMP to act as a sensor to control attachment and biofilm formation. When cyclic-di-GMP levels are high, LapD binds cyclic-di-GMP, triggering a conformational change that is communicated to the periplasmic domain through a HAMP domain, which then allows its periplasmic domain to bind the periplasmic protease LapG[53,54]. When cyclic-di-GMP levels drop, LapD is an unactive state, releasing LapG to cleave the LapA adhesin, allowing for biofilm detachment. Because of LapD's overall protein structure and its involvement with cyclic-di-GMP, we believe that STM3615 might work in a similar way through interactions with its periplasmic domain and a periplasmic protein partner.
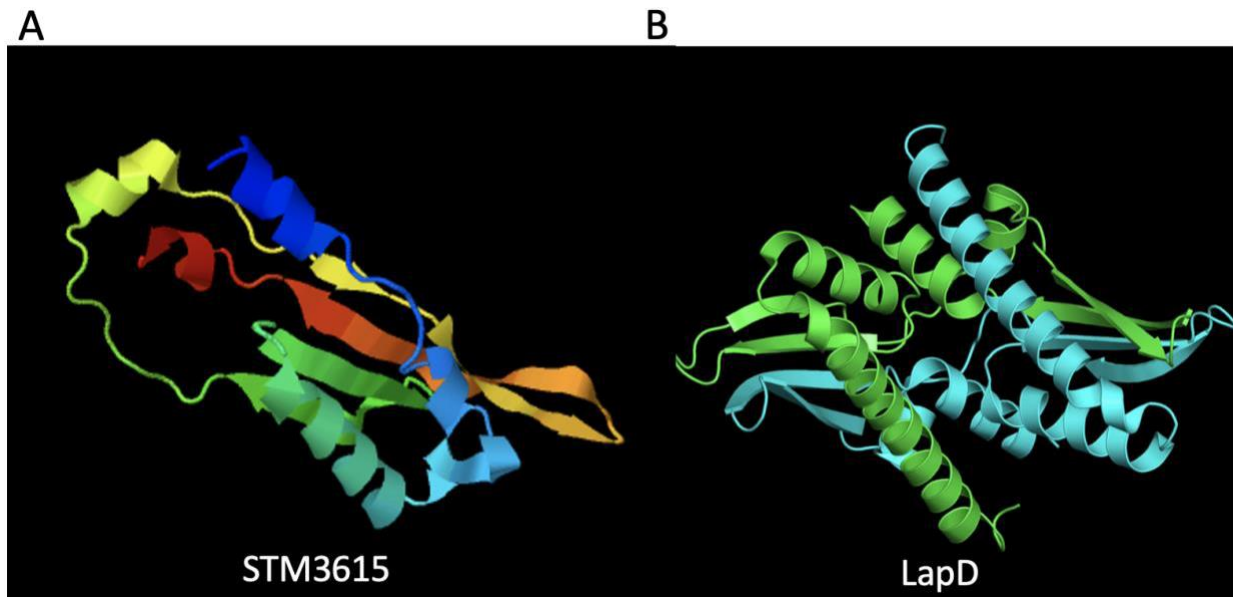
Fig. 19 Periplasmic domains of STM3615 and LapD
A) The predicted structure of STM3615's periplasmic domain according to PHYRE analysis. B) The closest match to STM3615's periplasmic domain was LapD's periplasmic domain. As LapD functions as a dimer (teal and green are each one monomer), the structure of STM3615 will also open up as part of a dimer.

<center>Transposon Mutagenesis</center>

Unfortunately, *S.* Typhimurium does not encode a homolog to the LapA periplasmic partner of LapD. In order to identify the possible periplasmic partner of STM3615, I proceeded with a transposon mutagenesis approach instead. Transposons are moveable pieces of DNA that insert themselves into the genome randomly, thus interrupting genes and the subsequent transcription and translation processes. A Mariner-based transposon vector that has a complete transposon system including both the transposase enzyme and transposon (Fig. 20) was used to mutagenize the ΔSTM3615 mutant, then plated to green phage plates to identify mutants. Because I wanted to disrupt the possible periplasmic domain partner, I selected colonies that reverted to the WT white phenotype on the green phage plates that were then grown up and the insertion site was amplified by PCR and sent for sequencing (Fig. 9, 10)[47].

Figure 21 shows the makeup of the sequencing results. 17 colonies came back with hits on identifiable interrupted genes. Several of these hits were mutants of the phosphotransferase system (PTS). The PTS has a range of functions, but its primary function is the catalysis of sugar transport, phosphorylation, and chemoreception[55]. Because the green phage plates contain glucose, PTS mutants were expected as false positives. When the transposon inserts itself into PTS genes (specifically *ptsI* and *ptsG* in this study), the bacterium is unable to transport the glucose present in the agar into the cell, resulting in a white colony instead of the green colony, indicative of glucose acidifying the cytoplasm. Six colonies had sequencing matching the transposon plasmid, indicating that the entire plasmid integrated into the genome instead of just the transposon or that these were spontaneously-resistant contaminating *E. coli* containing the transposon plasmid. Eight colonies came back with no sequencing results, indicating that the sequencing primer was unable to find the Rnd2-TnM20 in the PCR product. These colonies are

<center>48</center>

possibly spontaneous mutants that do not contain the transposon, although it is possible that an

alternative set of arbitrary primers might be able to identify their insertion sites. Further full

breakdown of transposon mutagenesis sequencing results can be found in Appendix D.
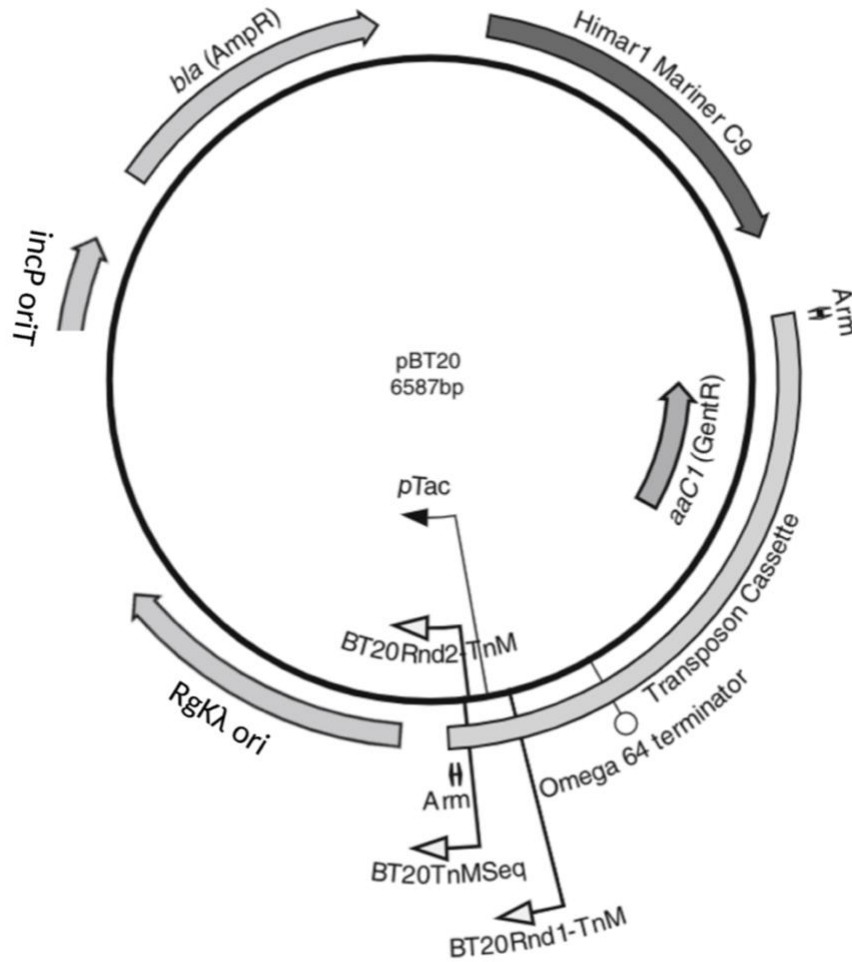
Fig. 20 pBT20 transposon vector genetic map
The transposon vector pBT20 was used in the transposon mutagenesis trials in this study. pBT20
is based on the hyperactive Himar1 Mariner C9 transposase. The backbone of the vector also
contains the bla gene which confers ampicillin resistance. The transposon cassette itself has two
outward facing promoters, pTac and p-aaC1, which allow for both over-expression and loss of
function for genes interrupted by the transposon. Gentamicin resistance is conferred in the
transposon through the aaC1 gene. To stop replication in recipient strains, a suicide vector R6Kλ
origin of replication is present in the plasmid.
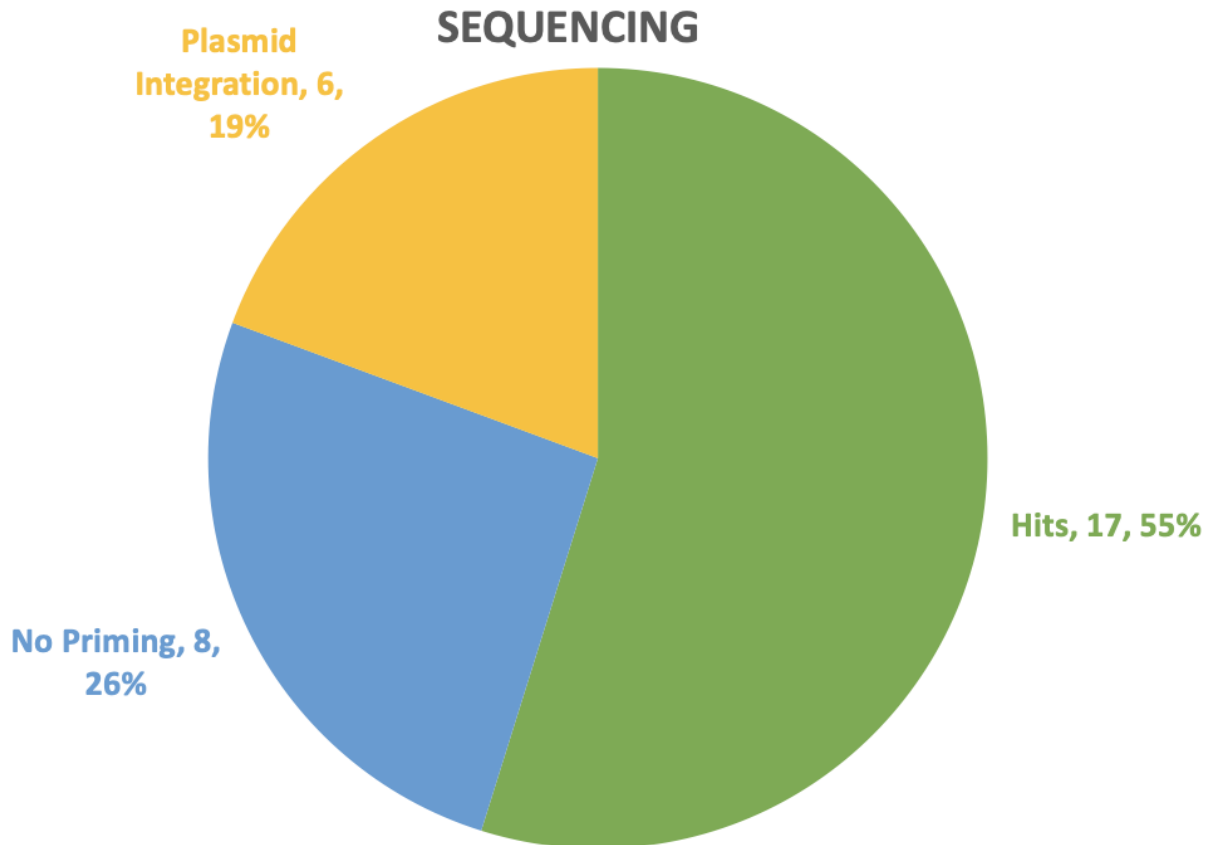
Fig. 21 Transposon mutagenesis sequencing results
31 colonies from the transposon mutagenesis trials that displayed a revertant white colony phenotype in the ΔSTM3615 background were able to be grown up and sequenced. 17 colonies were positive hits for *Salmonella* Typhimurium genes. Six colonies showed sequencing results of the plasmid itself, indicating entire plasmid integration or contaminating *E. coli* as opposed to the desired transposon integration. Eight colonies had the result of no priming, suggesting that they may be spontaneous mutants that do not contain the transposon as the transposon primers were unable to interact with them.

A22 Survival Assay Identifies *rcsD* and *yrfG* Transposon Mutants Revert the ΔSTM3615

Phenotype

Because of the stark difference in growth between wild type *S.* Typhimurium and

ΔSTM3615 on plates containing the MreB inhibitor A22 (Fig. 15), we decided to use A22 as a

way to test the transposon mutants to create a smaller group for further testing. I used the 10-fold

serial dilution 6x6 drop plate method as previously described on both LB and LB + A22 plates to

observe those ΔSTM3615 transposon mutants whose phenotype reverted to the WT growth

pattern. Two mutants had comparable growth on the antibiotic plates compared to the LB plates

(Fig. 22), so they were chosen to expand upon. The two mutants had interrupted genes of *rcsD*

and *yrfG*, respectfully. *rcsD* encodes for a transmembrane phosphotransferase component of the

larger Rcs phosphorelay system which regulates transcription of multiple genes[56–58], while *yrfG*

encodes for a purine nucleotidase of the haloacid dehalogenase (HAD)-like hydrolase

superfamily[59]. These two mutants were selected as prime candidates for future testing.
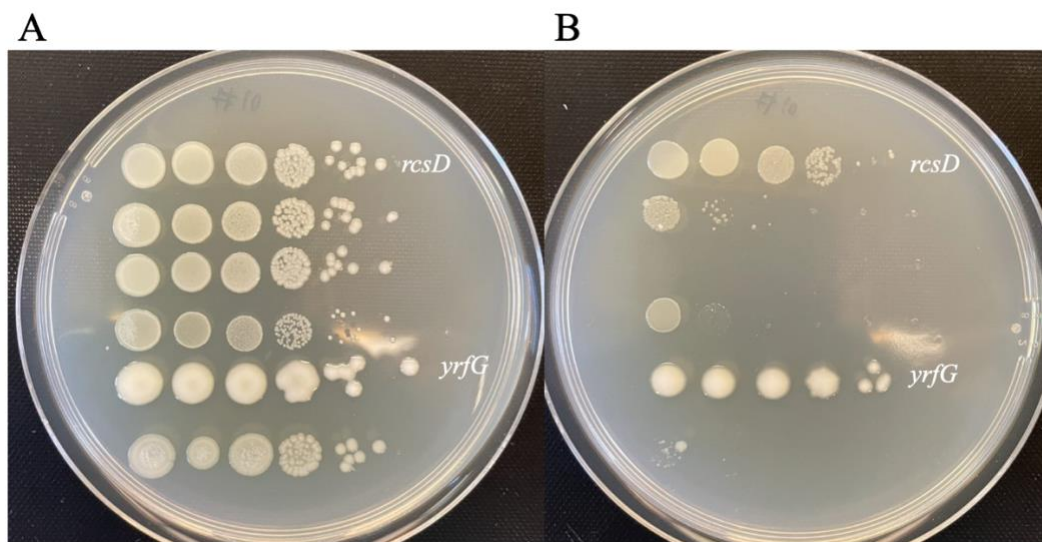
Fig. 22 Transposon mutants in *rcsD* and *yrfG* exhibit similar growth pattern to WT in presence
of A22 antibiotic
A) Six transposon mutants were plated on LB plates (A) or LB + A22 plates (B) in the 6x6 drop
plate method. Mutants of interest, *rcsD* and *yrfG*, can be seen in the first and fifth row
respectfully as having similar growth to their LB plate counterparts and to the WT in Figure 15.

CHAPTER 4. DISCUSSION

Previous studies identified a phenotype in the deletion mutant of the cyclic-di-GMP-specific phosphodiesterase STM3615 that is characterized by an increased rate of death on agar plates (Fig. 11) and a shortened bacterial rod length (Fig. 13). Here, we identified that the ΔSTM3615 deletion mutant also displayed a sensitivity to the inhibitor A22, a drug that targets the bacterial actin-like protein MreB that is responsible for proper bacterial morphology (Fig. 15). Testing with A22 determined that rather than the cyclic-di-GMP-specific phosphodiesterase activity, the uncharacterized periplasmic domain was responsible for the phenotype observed in the ΔSTM3615 deletion mutant. Following some bioinformatic analysis of the STM3615 protein, I hypothesized that the periplasmic domain of STM3615 has a periplasmic protein partner that is involved in the short bacterial length seen in the ΔSTM3615 mutant.

The amino acid sequence of the periplasmic domain was entered into PHYRE to discover any similarity with known crystallized proteins. The STM3615 periplasmic domain had the most similarity with LapD's periplasmic domain (Fig. 19). LapD is a cyclic-di-GMP-binding effector protein crystallized from *Pseudomonas fluorescens* Pf0–1 whose domain structure highly resembles that of STM3615, with the exception that the phosphodiesterase domain is inactivated in LapD[53]. LapD works through an inside-out signaling mechanism in which the protein has two states depending on its interaction with cyclic-di-GMP. When LapD binds cyclic-di-GMP, the protein undergoes a conformational change, allowing it to bind and sequester a periplasmic protease, LapG. When LapG is bound by LapD, it is unable to cleave its target, LapA, an adhesin. Free from cleavage, LapA is expressed on the surface where it assists the cell in attachment and biofilm formation. On the other hand, when cyclic-di-GMP levels drop and LapD's EAL domain does not bind cyclic-di-GMP, it stays in an autoinhibited state. In this state,

LapG is released to cleave the N-terminus of LapA, releasing it from the cell surface and contributing to cell detachment[53,54].

Because of the PHYRE results and LapD's structure and function, we hypothesized an STM3615 model based on LapD in which STM3615 interacts with a periplasmic protein through its periplasmic domain (Fig. 23). As long as the STM3615 periplasmic domain is present, it binds its periplasmic protein partner, allowing proper regulation of this phenotype. However, when the periplasmic domain is absent, in the case of the ΔSTM3615 and STM3615$_{\Delta peri}$ mutant, the periplasmic protein partner is no longer sequestered, causing this potential replication-involved length phenotype. While LapD's phosphodiesterase domain is inactive and regulation of periplasmic binding is tied to its ability to instead bind cyclic-di-GMP, the STM3615 phosphodiesterase domain still possesses activity. We tested a mutant that contained a site-directed mutation of the EAL domain at the genomic locus where the glutamic acid and leucine amino acids were replaced with alanines which blocks the enzymatic activity of the EAL domain[29]. This mutant did not express the deletion mutant phenotype, suggesting that phosphodiesterase activity is dispensable for this phenotype, although this result does not rule out that the phosphodiesterase activity may still be co-regulated with periplasmic binding to serve some other purpose. Instead, the periplasmic domain appears to solely be responsible for the ΔSTM3615 deletion phenotype, so I utilized transposon mutagenesis within the ΔSTM3615 mutant in an attempt to disrupt the protein partner.
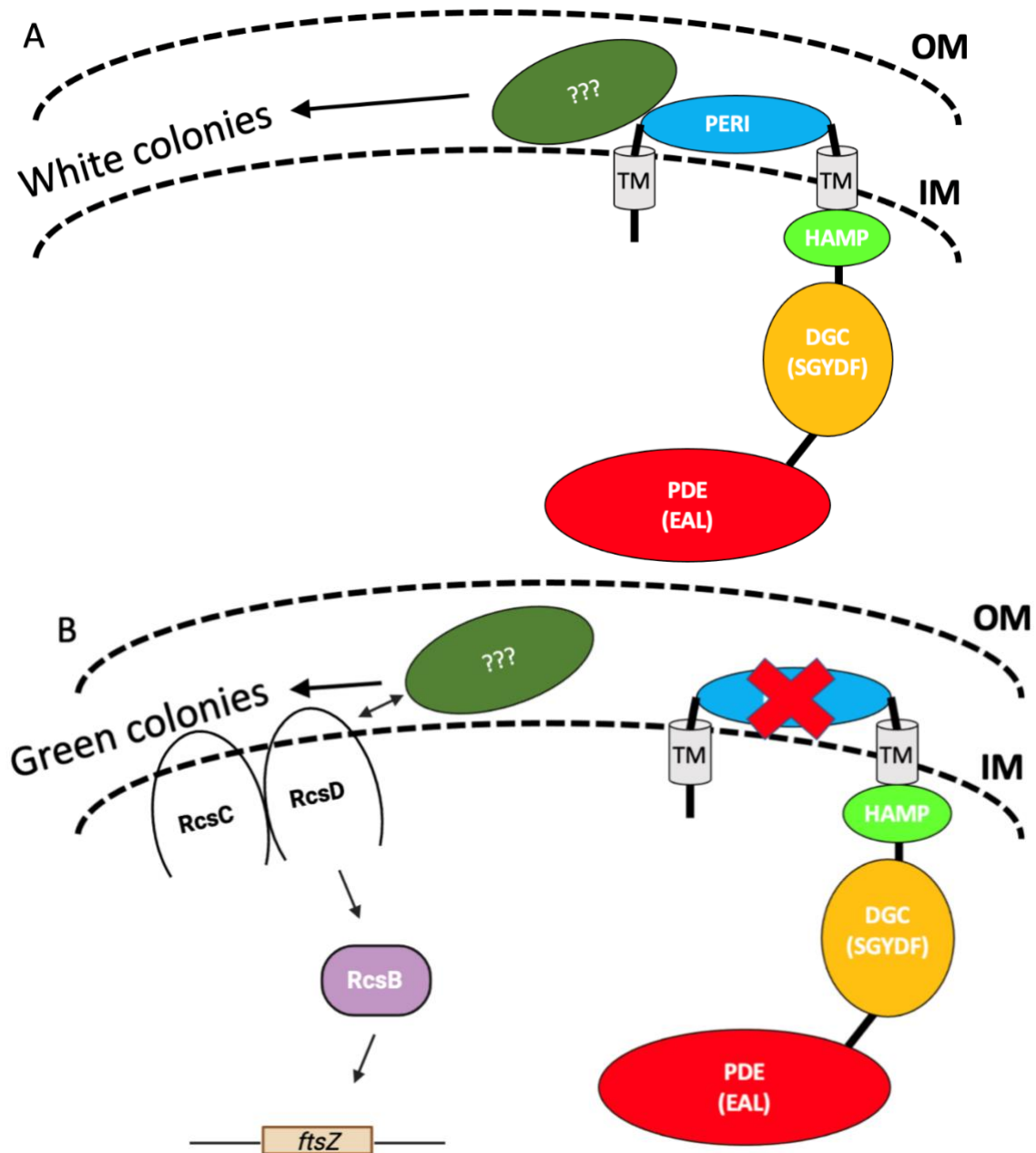
Fig. 23 Potential STM3615 model
A) When STM3615 and its periplasmic domain are intact, it can bind its periplasmic protein partner, creating the white colony phenotype on the green phage plates. B) When STM3615's periplasmic domain is absent, its periplasmic protein partner is able to enact its function, creating the green colony phenotype on the green phage plates. A simplified Rcs pathway diagram has been inserted into the model to depict the potential of its involvement in this mechanism. OM – outer membrane, IM – inner membrane.

Through the transposon mutagenesis trials, I was able to disrupt eight distinct genes. These transposon mutants were further examined by their survival on LB + A22 plates (Fig. 22). The ΔSTM3615 mutant is quite sensitive to A22 whereas WT is not (Fig. 15). Tn mutants that reverted the ΔSTM3615 phenotype to the wild type phenotype by surviving equally well on LB and LB + A22 plates were selected for further testing. Because the transposon I used was selected because of the promoters coming out from either side of the transposon – providing the opportunity to up-regulate a gene following insertion depending on the location – the genes disrupted in these Tn mutants will be deleted from WT for future testing.

The Tn mutants that reverted the ΔSTM3615 phenotype on A22 plates had insertions within the genes *rcsD* and *yrfG*. RcsD is a phosphotransferase within the Rcs phosphorelay system made up of several Rcs proteins that work together to regulate gene expression for biofilm formation, virulence, and cell surface remodeling[56,60,61]. The system starts when RcsF, an outer membrane lipoprotein, receives a stress signal. It has been shown to interact with both IgaA, a negative regulator, and RcsC to activate RcsC, a histidine kinase, to undergo autophosphorylation[62,63]. A phosphate group is passed from RcsC to RcsD, then onto the receiver domain of RcsB. This phosphorylated form of RcsB then goes on to homodimerize to regulate promoters for various genes including *osmC*, *ftsZ*, or the sRNA *rprA*. FtsZ is of particular interest as it is responsible for forming the Z ring that constricts the cell in the center to initiate division and is essential to the proper division of a bacterial cell[64].

In an experiment investigating the role RcsD has on RcsB, with the deletion of *rcsD*, the capsular polysaccharide synthesis (cps) genes that are regulated by RcsB were not active, even if RcsB was present[65]. Without the phosphorylation of RcsB by RcsD, RcsB cannot regulate its promotors, causing those genes to not be transcribed. While the disruption of *rcsD* by transposon

mutagenesis would inhibit RcsB's role in the regulation of *ftsZ*, *ftsZ*'s transcription would not be completely zero as there are other promotors of *ftsZ* that would continue initiating its transcription[58]. RcsB also regulates the promotor for *ftsA*, maintaining the necessary amounts of each protein. It has been shown that increased levels of *ftsA* and *ftsZ* activate cell division and lead to cells dividing earlier than they should, and overexpression of RcsB was shown to result in smaller cells[66]. The ΔSTM3615 mutant has a short length phenotype that might be the result of rapid division of the cell. The STM3615 periplasmic domain might work as a regulator of this process, and without it, the timing of the division process is impaired. By deleting RcsD and reducing the RcsB-mediated expression of FtsZ and FtsA, this may be restoring the balance to cell division.

The other gene disrupted by the transposon was *yrfG*. YrfG is a purine nucleotidase that is part of the larger haloacid dehalogenase (HAD)-like hydrolase family[59]. It is responsible for removing the phosphate groups from nucleotides – primarily the purines GMP and IMP – in the presence of Mg^{2+} [67]. Interestingly, there is a connection between RcsD and YrfG. *yrfG* is part of an operon that includes two heat shock proteins, YrfH and YrfI, as well as the negative regulator of the Rcs phosphorelay system, IgaA[68]. In times of cellular stress, IgaA interacts with RcsF to activate the Rcs phosphorelay system. Without that stress signal, IgaA interacts with RcsD, inhibiting its function, so that a phosphate group is unable to be passed from RcsC to RcsB to regulate gene expression[61]. In the IgaA/YrfG operon, the genes go in order from *igaA*, *yrfG*, *yrfH*, and *yrfI*, so while our transposon insertion into *yrfG* could inhibit the two genes downstream of it, it is less likely that IgaA would be inhibited[68]. Both YrfH and YrfI are chaperones though, so they could be involved in folding IgaA or another related protein. Deletion of *yrfG* would eliminate a purine nucleotidase, but it is unlikely that this would be

catastrophic as there is overlap in the substrates of HAD enzymes[67]. In particular, the nucleotidase NagD binds GMP just like YrfG[69]. It is possible that it is IgaA and not YrfG that is involved in this process. A disruption in IgaA would allow the Rcs pathway to become overactivated, resulting in more activation of promotors regulated by RcsB. Although it is unclear why overactivated RcsB would restore the ΔSTM3615 phenotype to wild type, it is possible that this tightly controlled system is sent out of whack by deleting STM3615 and further dysregulated by upregulating RcsB activity.

Because the periplasmic domain is the cause of the phenotypes seen by STM3615, we predicted that a periplasmic protein partner was interacting with it. In terms of the two genes, *rcsD* and *yrfG*, that were disrupted in the transposon mutagenesis in hopes of finding that potential periplasmic partner, it is unlikely that YrfG is the direct-binding periplasmic protein partner because it is not found in the periplasm. RcsD, on the other hand, does have a periplasmic domain that it uses to interact with IgaA[70]. Other proteins in the Rcs pathway that have periplasmic domains are RcsC and RcsF that could be potential partners for STM3615. By inhibiting RcsD through transposon mutagenesis, those two proteins would not necessarily be affected directly, but their function in the cell would not matter as the signal received by RcsF leading to the phosphate group of RcsC would not continue to its final destination of RcsB without the presence of RcsD[65]. The entire pathway must stay intact for its effect to be seen. In the *yrfG* operon, the only member that has a periplasmic domain is IgaA. Because *igaA* is upstream from *yrfG* in the operon, it is unlikely to be affected by the *yrfG* disruption by transposon mutagenesis, but it could still play a role in this mechanism.

Based on the findings of this thesis, there are many avenues of future research. First, we need to test the single gene deletions to determine whether a deletion mutant exhibits the same

phenotypes, and whether we can complement these mutants. This will also help to confirm

whether the *yrfG* mutant is operating through *yrfG* or through the neighboring *igaA*. To see if the

overproduction of FtsZ and FtsA are responsible for the phenotype, we could measure the

transcript levels for each gene through next-generation sequencing. Determining if IgaA is

physically interacting with either RcsF or RcsD in the presence of correct cellular signals would

help elucidate if the overactivation of the Rcs pathway is to blame. Further, observing these

mutants under a microscope to determine their morphology is necessary to compare the results to

the ΔSTM3615 mutant and WT. Additional transposon mutagenesis trials could be conducted to

increase the diversity of genes investigated. Next, for both proteins identified in the transposon

assay and other proteins of interest involved in their pathways, a bacterial two-hybrid system

could be set up to investigate direct protein-protein interactions[71]. Further, because the

periplasmic protein partner might be involved in replication, it might be encoded by an essential

gene which means it will be unable to be detected in a transposon mutagenesis screen as the

strain would simply not grow. To account for this, the bacterial two-hybrid system could be

expanded to all proteins and tested on their physical interaction with STM3615's periplasmic

domain. Through additional research, the periplasmic protein partner could be identified which

would allow us to expand our investigation of the STM3615 morphology pathway.

<div align="center">Conclusion</div>

The ΔSTM3615 mutant's length phenotype could be caused by impaired regulation of

replication. Through the exploration of this phenotype and its cause, more about *Salmonella*

regulation of replication could be uncovered, leading to a better understanding of these

regulatory systems. The periplasmic domain of STM3615 was found to be involved in the length

phenotype that also exhibited increased sensitivity to the MreB inhibitor A22, implying a

potential link to cell replication. The fact that STM3615, unlike the similarly organized LapD, retains cyclic-di-GMP phosphodiesterase activity may also suggest a connection to cyclic-di-GMP regulation.

This study started the process of identifying the periplasmic protein partner of STM3615. Through transposon mutagenesis, potential pathway components have been identified as RcsD and YrfG. Further investigation of the disrupted genes found and their physical interaction with STM3615 is needed. Because of STM3615's potential involvement in the essential process of bacterial replication, more investigation is required to put together the full mechanism behind the ΔSTM3615 mutant's phenotypes. More exploration of *Salmonella's* replication mechanisms could elucidate novel therapies to help in the fight against increasing bacterial antibiotic resistance.

REFERENCES

1. Jajere SM. A review of Salmonella enterica with particular focus on the pathogenicity and virulence factors, host specificity and antimicrobial resistance including multidrug resistance. Veterinary World. 2019;12(4):504–521. doi:10.14202/vetworld.2019.504-521

2. Fàbrega A, Vila J. Salmonella enterica Serovar Typhimurium Skills To Succeed in the Host: Virulence and Regulation. Clinical Microbiology Reviews. 2013;26(2):308–341. doi:10.1128/CMR.00066-12

3. Galán JE. Salmonella Typhimurium and inflammation: a pathogen-centric affair. Nature reviews. Microbiology. 2021;19(11):716–725. doi:10.1038/s41579-021-00561-4

4. Majowicz SE, Musto J, Scallan E, Angulo FJ, Kirk M, O'Brien SJ, Jones TF, Fazil A, Hoekstra RM, International Collaboration on Enteric Disease "Burden of Illness" Studies. The global burden of nontyphoidal Salmonella gastroenteritis. Clinical Infectious Diseases: An Official Publication of the Infectious Diseases Society of America. 2010;50(6):882–889. doi:10.1086/650733

5. Coburn B, Grassl GA, Finlay BB. Salmonella, the host and disease: a brief review. Immunology & Cell Biology. 2007;85(2):112–118. doi:10.1038/sj.icb.7100007

6. Crump JA, Sjölund-Karlsson M, Gordon MA, Parry CM. Epidemiology, Clinical Presentation, Laboratory Diagnosis, Antimicrobial Resistance, and Antimicrobial Management of Invasive Salmonella Infections. Clinical Microbiology Reviews. 2015;28(4):901–937. doi:10.1128/CMR.00002-15

7. Nilsson OR, Kari L, Steele-Mortimer O. Foodborne infection of mice with Salmonella Typhimurium. PLoS ONE. 2019;14(8):e0215190. doi:10.1371/journal.pone.0215190

8. Broz P, Ohlson MB, Monack DM. Innate immune response to Salmonella typhimurium, a model enteric pathogen. Gut microbes. 2012;3(2):62–70. doi:10.4161/gmic.19141

9. Kysela DT, Randich AM, Caccamo PD, Brun YV. Diversity Takes Shape: Understanding the Mechanistic and Adaptive Basis of Bacterial Morphology. PLoS Biology. 2016;14(10):e1002565. doi:10.1371/journal.pbio.1002565

10. Young KD. The Selective Value of Bacterial Shape. Microbiology and Molecular Biology Reviews. 2006;70(3):660–703. doi:10.1128/mmbr.00001-06

11. van Teeseling MCF, de Pedro MA, Cava F. Determinants of Bacterial Morphology: From Fundamentals to Possibilities for Antimicrobial Targeting. Frontiers in Microbiology. 2017 [accessed 2023 Jun 20];8. https://www.frontiersin.org/articles/10.3389/fmicb.2017.01264

12. Randich AM, Brun YV. Molecular mechanisms for the evolution of bacterial morphologies and growth modes. Frontiers in Microbiology. 2015;6:580. doi:10.3389/fmicb.2015.00580

13. Vollmer W, Blanot D, De Pedro MA. Peptidoglycan structure and architecture. FEMS Microbiology Reviews. 2008;32(2):149–167. doi:10.1111/j.1574-6976.2007.00094.x

14. Wachi M, Doi M, Okada Y, Matsuhashi M. New mre genes mreC and mreD, responsible for formation of the rod shape of Escherichia coli cells. Journal of Bacteriology. 1989;171(12):6511–6516.

15. Jones LJF, Carballido-López R, Errington J. Control of Cell Shape in Bacteria: Helical, Actin-like Filaments in Bacillus subtilis. Cell. 2001;104(6):913–922. doi:10.1016/S0092-8674(01)00287-2

16. Hamill PG, Stevenson A, McMullan PE, Williams JP, Lewis ADR, S S, Stevenson KE, Farnsworth KD, Khroustalyova G, Takemoto JY, et al. Microbial lag phase can be indicative of, or independent from, cellular stress. Scientific Reports. 2020;10(1):5948. doi:10.1038/s41598-020-62552-4

17. Jun S, Si F, Pugatch R, Scott M. Fundamental Principles in Bacterial Physiology - History, Recent progress, and the Future with Focus on Cell Size Control: A Review. Reports on progress in physics. Physical Society (Great Britain). 2018;81(5):056601. doi:10.1088/1361-6633/aaa628

18. Finkel SE. Long-term survival during stationary phase: evolution and the GASP phenotype. Nature Reviews Microbiology. 2006;4(2):113–120. doi:10.1038/nrmicro1340

19. Römling U, Galperin MY, Gomelsky M. Cyclic di-GMP: the First 25 Years of a Universal Bacterial Second Messenger. Microbiology and Molecular Biology Reviews : MMBR. 2013;77(1):1–52. doi:10.1128/MMBR.00043-12

20. Ryan RP. Cyclic di-GMP signalling and the regulation of bacterial virulence. Microbiology. 2013;159(Pt 7):1286–1297. doi:10.1099/mic.0.068189-0

21. Hall CL, Lee VT. Cyclic-di-GMP regulation of virulence in bacterial pathogens. Wiley interdisciplinary reviews. RNA. 2018;9(1):10.1002/wrna.1454. doi:10.1002/wrna.1454

22. Jenal U, Reinders A, Lori C. Cyclic di-GMP: second messenger extraordinaire. Nature Reviews Microbiology. 2017;15(5):271–284. doi:10.1038/nrmicro.2016.190

23. Ryan RP, Tolker-Nielsen T, Dow JM. When the PilZ don't work: effectors for cyclic di-GMP action in bacteria. Trends in Microbiology. 2012;20(5):235–242. doi:10.1016/j.tim.2012.02.008

24. Lori C, Ozaki S, Steiner S, Böhm R, Abel S, Dubey BN, Schirmer T, Hiller S, Jenal U. Cyclic di-GMP acts as a cell cycle oscillator to drive chromosome replication. Nature. 2015;523(7559):236–239. doi:10.1038/nature14473

25. Hermanas TM, Subramanian S, Dann CE, Stewart GC. Spore-Associated Proteins Involved in c-di-GMP Synthesis and Degradation of Bacillus anthracis. Journal of Bacteriology. 203(17):e00135-21. doi:10.1128/JB.00135-21

26. Skotnicka D, Smaldone GT, Petters T, Trampari E, Liang J, Kaever V, Malone JG, Singer M, Søgaard-Andersen L. A Minimal Threshold of c-di-GMP Is Essential for Fruiting Body Formation and Sporulation in Myxococcus xanthus. PLoS Genetics. 2016;12(5):e1006080. doi:10.1371/journal.pgen.1006080

27. Gallagher KA, Schumacher MA, Bush MJ, Bibb MJ, Chandra G, Holmes NA, Zeng W, Henderson M, Zhang H, Findlay KC, et al. c-di-GMP Arms an Anti-σ to Control Progression of Multicellular Differentiation in Streptomyces. Molecular Cell. 2020;77(3):586-599.e6. doi:10.1016/j.molcel.2019.11.006

28. Edwards AN, Willams CL, Pareek N, McBride SM, Tamayo R. c-di-GMP Inhibits Early Sporulation in Clostridioides difficile. mSphere. 6(6):e00919-21. doi:10.1128/msphere.00919-21

29. Petersen E, Mills E, Miller SI. Cyclic-di-GMP regulation promotes survival of a slow-replicating subpopulation of intracellular Salmonella Typhimurium. Proceedings of the National Academy of Sciences of the United States of America. 2019;116(13):6335–6340. doi:10.1073/pnas.1901051116

30. Rosseto FR. Estudos estruturais e funcionais de STM3615 de Salmonella enterica: uma proteína contendo ambos os domínios GGDEF-EAL envolvidos na biossíntese de c-di-GMP [text]. Universidade de São Paulo; 2016. http://www.teses.usp.br/teses/disponiveis/76/76132/tde-23032017-093752/. doi:10.11606/T.76.2017.tde-23032017-093752

31. Matamouros S, Hager KR, Miller SI. HAMP Domain Rotation and Tilting Movements Associated with Signal Transduction in the PhoQ Sensor Kinase. mBio. 2015;6(3):e00616-15. doi:10.1128/mBio.00616-15

32. Chen L-H, Köseoğlu VK, Güvener ZT, Myers-Morales T, Reed JM, D'Orazio SEF, Miller KW, Gomelsky M. Cyclic di-GMP-dependent Signaling Pathways in the Pathogenic Firmicute Listeria monocytogenes. PLoS Pathogens. 2014;10(8):e1004301. doi:10.1371/journal.ppat.1004301

33. Stewart MK, Cummings LA, Johnson ML, Berezow AB, Cookson BT. Regulation of phenotypic heterogeneity permits Salmonella evasion of the host caspase-1 inflammatory response. Proceedings of the National Academy of Sciences of the United States of America. 2011;108(51):20742–20747. doi:10.1073/pnas.1108963108

34. Yang H-J, Bogomolnaya LM, Elfenbein JR, Endicott-Yazdani T, Reynolds MM, Porwollik S, Cheng P, Xia X-Q, McClelland M, Andrews-Polymenis H. Novel Two-Step Hierarchical Screening of Mutant Pools Reveals Mutants under Selection in Chicks. Infection and Immunity. 2016;84(4):1226–1238. doi:10.1128/IAI.01525-15

35. Ahmad I, Lamprokostopoulou A, Le Guyon S, Streck E, Barthel M, Peters V, Hardt W-D, Römling U. Complex c-di-GMP Signaling Networks Mediate Transition between Virulence Properties and Biofilm Formation in Salmonella enterica Serovar Typhimurium Webber MA, editor. PLoS ONE. 2011;6(12):e28351. doi:10.1371/journal.pone.0028351

36. Anwar N, Rouf SF, Römling U, Rhen M. Modulation of Biofilm-Formation in Salmonella enterica Serovar Typhimurium by the Periplasmic DsbA/DsbB Oxidoreductase System Requires the GGDEF-EAL Domain Protein STM3615. PLoS ONE. 2014;9(8):e106095. doi:10.1371/journal.pone.0106095

37. Chen CY, Nace GW, Irwin PL. A 6 x 6 drop plate method for simultaneous colony counting and MPN enumeration of Campylobacter jejuni, Listeria monocytogenes, and Escherichia coli. Journal of Microbiological Methods. 2003;55(2):475–479. doi:10.1016/s0167-7012(03)00194-5

38. Mills E, Petersen E, Kulasekara BR, Miller SI. A direct screen for c-di-GMP modulators reveals a Salmonella Typhimurium periplasmic ʟ-arginine–sensing pathway. Science Signaling. 2015;8(380):ra57–ra57. doi:10.1126/scisignal.aaa1796

39. Ducret A, Quardokus EM, Brun YV. MicrobeJ, a tool for high throughput bacterial cell detection and quantitative analysis. Nature Microbiology. 2016;1(7):1–7. doi:10.1038/nmicrobiol.2016.77

40. Caldwell BJ, Bell CE. Structure and mechanism of the Red recombination system of bacteriophage λ. Progress in Biophysics and Molecular Biology. 2019;147:33–46. (The Structural Biology of DNA Response and Repair). doi:10.1016/j.pbiomolbio.2019.03.005

41. Ebel-Tsipis J, Botstein D, Fox MS. Generalized transduction by phage P22 in Salmonella typhimurium: I. Molecular origin of transducing DNA. Journal of Molecular Biology. 1972;71(2):433–448. doi:10.1016/0022-2836(72)90361-0

42. Letunic I, Bork P. 20 years of the SMART protein domain annotation resource. Nucleic Acids Research. 2018;46(D1):D493–D496. doi:10.1093/nar/gkx922

43. Letunic I, Khedkar S, Bork P. SMART: recent updates, new developments and status in 2020. Nucleic Acids Research. 2021;49(D1):D458–D460. doi:10.1093/nar/gkaa937

44. Lu S, Wang J, Chitsaz F, Derbyshire MK, Geer RC, Gonzales NR, Gwadz M, Hurwitz DI, Marchler GH, Song JS, et al. CDD/SPARCLE: the conserved domain database in 2020. Nucleic Acids Research. 2020;48(D1):D265–D268. doi:10.1093/nar/gkz991

45. Kelley LA, Mezulis S, Yates CM, Wass MN, Sternberg MJE. The Phyre2 web portal for protein modeling, prediction and analysis. Nature Protocols. 2015;10(6):845–858. doi:10.1038/nprot.2015.053

46. Gunn JS, Alpuche-Aranda CM, Loomis WP, Belden WJ, Miller SI. Characterization of the Salmonella typhimurium pagC/pagD chromosomal region. Journal of Bacteriology. 1995;177(17):5040–5047. doi:10.1128/jb.177.17.5040-5047.1995

47. Kulasekara HD. Transposon Mutagenesis. In: Filloux A, Ramos J-L, editors. Pseudomonas Methods and Protocols. New York, NY: Springer; 2014. p. 501–519. (Methods in Molecular Biology). https://doi.org/10.1007/978-1-4939-0473-0_39. doi:10.1007/978-1-4939-0473-0_39

48. Altschul SF, Gish W, Miller W, Myers EW, Lipman DJ. Basic local alignment search tool. Journal of Molecular Biology. 1990;215(3):403–410. doi:10.1016/S0022-2836(05)80360-2

49. Yang C-Y, Chin K-H, Chuah ML-C, Liang Z-X, Wang AH-J, Chou S-H. The structure and inhibition of a GGDEF diguanylate cyclase complexed with (c-di-GMP)(2) at the active site. Acta Crystallographica. Section D, Biological Crystallography. 2011;67(Pt 12):997–1008. doi:10.1107/S090744491104039X

50. Sundriyal A, Massa C, Samoray D, Zehender F, Sharpe T, Jenal U, Schirmer T. Inherent Regulation of EAL Domain-catalyzed Hydrolysis of Second Messenger Cyclic di-GMP. The Journal of Biological Chemistry. 2014;289(10):6978–6990. doi:10.1074/jbc.M113.516195

51. Awuni E, Mu Y. Effect of A22 on the Conformation of Bacterial Actin MreB. International Journal of Molecular Sciences. 2019;20(6):1304. doi:10.3390/ijms20061304

52. Iwai N, Nagai K, Wachi M. Novel S-benzylisothiourea compound that induces spherical cells in Escherichia coli probably by acting on a rod-shape-determining protein(s) other than penicillin-binding protein 2. Bioscience, Biotechnology, and Biochemistry. 2002;66(12):2658–2662. doi:10.1271/bbb.66.2658

53. Newell PD, Monds RD, O'Toole GA. LapD is a bis-(3',5')-cyclic dimeric GMP-binding protein that regulates surface attachment by Pseudomonas fluorescens Pf0-1. Proceedings of the National Academy of Sciences. 2009;106(9):3461–3466. doi:10.1073/pnas.0808933106

54. Newell PD, Boyd CD, Sondermann H, O'Toole GA. A c-di-GMP Effector System Controls Cell Adhesion by Inside-Out Signaling and Surface Protein Cleavage. PLoS Biology. 2011;9(2):e1000587. doi:10.1371/journal.pbio.1000587

55. Postma PW, Lengeler JW, Jacobson GR. Phosphoenolpyruvate:carbohydrate phosphotransferase systems of bacteria. Microbiological Reviews. 1993;57(3):543–594.

56. Erickson KD, Detweiler CS. The Rcs phosphorelay system is specific to enteric pathogens/commensals and activates ydeI, a gene important for persistent Salmonella infection of mice. Molecular Microbiology. 2006;62(3):883–894. doi:10.1111/j.1365-2958.2006.05420.x

57. Guo X-P, Sun Y-C. New Insights into the Non-orthodox Two Component Rcs Phosphorelay System. Frontiers in Microbiology. 2017;8:2014. doi:10.3389/fmicb.2017.02014

58. Majdalani N, Gottesman S. THE RCS PHOSPHORELAY: A Complex Signal Transduction System. Annual Review of Microbiology. 2005;59(1):379–405. doi:10.1146/annurev.micro.59.050405.101230

59. Terakawa A, Natsume A, Okada A, Nishihata S, Kuse J, Tanaka K, Takenaka S, Ishikawa S, Yoshida K. Bacillus subtilis 5′-nucleotidases with various functions and substrate specificities. BMC Microbiology. 2016;16:249. doi:10.1186/s12866-016-0866-5

60. Clarke DJ. The Rcs phosphorelay: more than just a two-component pathway. Future Microbiology. 2010;5(8):1173–1184. doi:10.2217/fmb.10.83

61. Wall E, Majdalani N, Gottesman S. The Complex Rcs Regulatory Cascade. Annual Review of Microbiology. 2018;72(1):111–139. doi:10.1146/annurev-micro-090817-062640

62. Meng J, Young G, Chen J. The Rcs System in Enterobacteriaceae: Envelope Stress Responses and Virulence Regulation. Frontiers in Microbiology. 2021 [accessed 2023 Jun 27];12. https://www.frontiersin.org/articles/10.3389/fmicb.2021.627104

63. Sato T, Takano A, Hori N, Izawa T, Eda T, Sato K, Umekawa M, Miyagawa H, Matsumoto K, Muramatsu-Fujishiro A, et al. Role of the inner-membrane histidine kinase RcsC and outer-membrane lipoprotein RcsF in the activation of the Rcs phosphorelay signal transduction system in Escherichia coli. Microbiology. 2017;163(7):1071–1080. doi:10.1099/mic.0.000483

64. Erickson HP, Anderson DE, Osawa M. FtsZ in Bacterial Cytokinesis: Cytoskeleton and Force Generator All in One. Microbiology and Molecular Biology Reviews : MMBR. 2010;74(4):504–528. doi:10.1128/MMBR.00021-10

65. Takeda S, Fujisawa Y, Matsubara M, Aiba H, Mizuno T. A novel feature of the multistep phosphorelay in Escherichia coli: a revised model of the RcsC → YojN → RcsB signalling pathway implicated in capsular synthesis and swarming behaviour. Molecular Microbiology. 2001;40(2):440–450. doi:10.1046/j.1365-2958.2001.02393.x

66. Carballès F, Bertrand C, Bouché J-P, Cam K. Regulation of Escherichia coli cell division genes ftsA and ftsZ by the two-component system rcsC–rcsB. Molecular Microbiology. 1999;34(3):442–450. doi:10.1046/j.1365-2958.1999.01605.x

67. Kuznetsova E, Proudfoot M, Gonzalez CF, Brown G, Omelchenko MV, Borozan I, Carmel L, Wolf YI, Mori H, Savchenko AV, et al. Genome-wide Analysis of Substrate Specificities of the Escherichia coli Haloacid Dehalogenase-like Phosphatase Family*. Journal of Biological Chemistry. 2006;281(47):36149–36161. doi:10.1074/jbc.M605449200

68. García-Calderón CB, Casadesús J, Ramos-Morales F. Regulation of igaA and the Rcs System by the MviA Response Regulator in Salmonella enterica. Journal of Bacteriology. 2009;191(8):2743–2752. doi:10.1128/JB.01519-08

69. Tremblay LW, Dunaway-Mariano D, Allen KN. Structure and Activity Analyses of Escherichia coli K-12 NagD Provide Insight into the Evolution of Biochemical Function in the Haloalkanoic Acid Dehalogenase Superfamily,. Biochemistry. 2006;45(4):1183–1193. doi:10.1021/bi051842j

70. Wall EA, Majdalani N, Gottesman S. IgaA negatively regulates the Rcs Phosphorelay via contact with the RcsD Phosphotransfer Protein. PLoS Genetics. 2020;16(7):e1008610. doi:10.1371/journal.pgen.1008610

71. Battesti A, Bouveret E. The bacterial two-hybrid system based on adenylate cyclase reconstitution in Escherichia coli. Methods. 2012;58(4):325–334. (The Yeast two-hybrid system). doi:10.1016/j.ymeth.2012.07.018

72. Hammer BK, Swanson MS. Co-ordination of Legionella pneumophila virulence with entry into stationary phase by ppGpp. Molecular Microbiology. 1999;33(4):721–731. doi:10.1046/j.1365-2958.1999.01519.x

73. Datsenko KA, Wanner BL. One-step inactivation of chromosomal genes in Escherichia coli K-12 using PCR products. Proceedings of the National Academy of Sciences of the United States of America. 2000;97(12):6640–6645.

APPENDICES

Appendix A. Strains

Table 1 Strains used in this study

Strain	Genotype	Source
14028s	Wild-type *Salmonella enterica* subsp. e*nterica* (ex Kauffman and Edwards) Le Minor and Popoff serovar Typhimurium	ATCC®
EPST038	Δ*STM3615*::Cam	[38]
SM10-pBT20	pBT20	[47]
EPST050	Δ*STM3615::*Cam, pMMBAmp-*3615RBS*	This study
EPST198	*STM3615$_{AAA}$*::Kan	[29]
EPST243	*STM3615$_{Δperi}$*::Kan	This study
EPST247	*ΔSTM3615*::Cam, pBAD-*3615$_{FreePeri}$*	This study
EPST073	Δ*STM3615::*Cam, pMMBAmp-*3615$_{AAA}$*	This study
LPST001	*rcsD*::Kan	This study
LPST002	*yrfG*::Kan	This study
DH5α	DH5α	Invitrogen™

Table 2 Plasmids used in this study

Name	Vector	Antibiotic Resistance	Source
pEP256	pTopo	Kanamycin/Ampicillin	Invitrogen™
pEP236	pTopo-3615RBS	Kanamycin/Ampicillin	This study
pMMBA	pMMB67EH	Ampicillin	[72]
pUC19	pUC19	Ampicillin	Thermo Scientific™
pEP306	pUC19-Kan (pUCK)	Kanamycin/Ampicillin	This study
pEP240	pMMBA-3615RBS	Ampicillin	This study
pBAD24	pBAD24	Ampicillin	ATCC®
pEP347	pBAD-3615$_{FreePeri}$	Ampicillin	This study
pEP254	pMMBA-3615$_{AAA}$	Ampicillin	This study
pKD4	pKD4	Kanamycin/Ampicillin	[73]
pKD46	pKD46	Ampicillin	[73]

Appendix C. Oligonucleotides

Table 3 Oligonucleotides used in this study

Primer Name	Sequence	Purpose
Rnd1-ARB1-Pa	GGCCACGCGTCGACTAGTAC NNNNNNNNNNAGAG	Arbitrary primer for sequencing transposon insertions
Rnd1-ARB2-Pa	GGCCACGCGTCGACTAGTAC NNNNNNNNNNACGCC	Arbitrary primer for sequencing transposon insertions
Rnd1-ARB3-Pa	GGCCACGCGTCGACTAGTAC NNNNNNNNNNGATAT	Arbitrary primer for sequencing transposon insertions
Rnd1-ARB4-Pa	GGCCACGCGTCGACTAGTAC SNNNNNNNSNSSSGCG	Arbitrary primer for sequencing transposon insertions
Rnd2-ARB	GGCCACGCGTCGACTAGTAC	Second round primer for transposon insertion, anneals to Rnd1-ARB
Rnd1-TnM20	TATAATGTGTGGAATTGTGAGCGG	Rnd1 pBT20 transposon-specific PCR primer
Rnd2-TnM20	ACAGGAAACAGGACTCTAGAGG	Rnd2 pBT20 transposon-specific PCR primer
Seq-TnM20	CACCCAGCTTTCTTGTACAC	Sequencing transposon-specific PCR primer for pBT20
3615Comp RBS F	<u>GAA TTC</u> CAG GGA GAG TCA ATT TGC G	Primer to include native RBS in 3615 expression construct
3615Comp R	<u>AAG CTT</u> TTA ACT TTT GTA ATC AGG ATT TTC G	Primer to clone 3615 into pMMB expression vector
3615 noPeri Fwd (NheI)	ATA TTA <u>GCT AGC</u> GTC ATG AGC GCG CTC	Primer to delete periplasmic region of 3615, leaving the two TM regions
3615 noPeri Rvs (NheI)	ATA TTA <u>GCT AGC</u> GCG GTT CTG CTG TAC C	Primer to delete periplasmic region of 3615, leaving the two TM regions
pUC19 Kan Fwd (SalI)	ATA TTA <u>GTC GAC G</u>TG TAG GCT GGA GCT GCT TC	Primer to clone Kan from pKD4 into PUC vector for integration fragments
pUC19 Kan Rvs (HindIII)	ATA TTA <u>AAG CTT</u> CAT ATG AAT ATC CCT CCT TAG	Primer to clone Kan from pKD4 into PUC vector for integration fragments
3615 pBAD Comp Fwd (EcoRI)	ATA TTA <u>GAA TTC</u> TTG CGC GTC AGC C	Primer to amplify 3615RBS fragment and mutants for

		pBAD cloning and ara-inducible expression
3615SDM Int 3' Rvs (SalI)	ATA TTA <u>GTC GAC</u> TTA ACT TTT GTA ATC AGG ATT TTC GTG	Primer to clone 3' half of 3615 with DSM site into pUC vector for integration
3615Peri Integration LR Fwd	ATA CTC AGG CGG CAG TCC GGG ATA TCC AGG GAG AGT CAA T<u>TT</u> <u>GCG CGT</u> <u>CAG CCG CGC GTT</u>	Primer to generate LR fragment from pUCK-3615Peri
3615 LambdaRed Rvs	TTA ACT TTT GTA ATC AGG ATT TTC GTG CGA CAG ATA CCG TTC TTC AAA GAT CAT ATG AAT ATC CTC CTT AG	Primer to generate LR fragment from pUCK-3615Peri
3615Peri-PagC Fwd (EcoRI)	ATA TTA <u>GAA TTC </u>ATG AAA AAT ATT ATT TTA TCC ACT TTA GTT ATT ACT ACA AGC GTT TTG GTT GTA AAT GTT GCA CAG GCC GAT CAG CAG AAC CGC TAC AAC ACG GC	Long primer to clone 3615 periplasmic domain only with PagC signal sequence into pBAD
3615Peri-PagC Rvs (HindIII)	ATA TTA <u>AAG CTT</u> CGC GCT CAT GAC GAA CTT GTA C	Primer to clone 3615 periplasmic domain only with PagC signal sequence into pBAD

Appendix D. Transposon Mutants

Table 4 Transposon mutants used in this study

Number*	Sequencing Result	LB Growth Score[a]	A22 Growth Score[b]	Position of Insertion
1.1	*ptsI*	5	2	2597606
1.2	*ptsI*	5	2	2597632
1B	*glnA*	5	2	4230131
2	*rcsD*	5	3	242078
3	No priming	5	3	
4	*ptsI*	5	1	2597400
5	*yncB*	5	1	1687712
6	*rcsD*	5	5	2421176
7A	*hcr*	5	2	970967
7B	Plasmid sequence	5	1	
8	Plasmid sequence	5	2	
9	*yrfG*	6	5	3666454
10	Plasmid sequence	5	1	
11	*ptsI*	5	1	2597613
12	*ptsI*	5	1	2597608
13	*safD*	5	1	346916
14	*ptsI*	5	1	2597677
15	*ptsG*	6	2	1245207
17	No priming	4	3	
18	Plasmid sequence	4	1	
20	No priming	3	3	
21	Plasmid sequence	3	1	
24	*hcr*	2	2	970956
26	No priming	4	1	
27	*safD*	1	2	346908
29	Plasmid sequence	4	3	
30	No priming	4	3	
33	No priming	2	1	
34	No priming	4	3	
36	No priming	4	4	
37	*hcr*	4	4	970967

*Excluded transposon mutants that did not grow up in liquid culture following their removal from the original green plates

[a]The number of columns in a serial dilution that the strain grew on LB plates; the greater the number, the more the growth at higher dilutions

[b]The number of columns in a serial dilution that the strain grew on LB plates with a concentration of 2 µg/mL of A22 antibiotic; the greater the number, the more the growth at higher dilutions

VITA

ALEXANDRA PULLIAM

Education:	M.S. Biology-Microbiology Concentration, East Tennessee State University, Johnson City, Tennessee, 2023
	B.S. Biology, University of Alabama, Tuscaloosa, Alabama, 2021
	B.S. Psychology, University of Alabama, Tuscaloosa, Alabama, 2021
Professional Experience:	Graduate Assistant, East Tennessee State University, College of Health Sciences, 2021-2023
Presentations:	Identification of the Protein Components in a Periplasmic Mechanism Regulating Bacterial Morphology (2022), ETSU Biology Seminar
	Identification of the Protein Components in a Periplasmic Mechanism Regulating Bacterial Morphology (2023), ETSU Biology Seminar
Honors and Awards:	Graduate School Research Grant, East Tennessee State University, 2022